

CERN-EP-2021-117
2021/12/30

CMS-TOP-18-010

Measurement of the inclusive and differential $t\bar{t}\gamma$ cross sections in the single-lepton channel and EFT interpretation at $\sqrt{s} = 13$ TeV

The CMS Collaboration*

Abstract

The production cross section of a top quark pair in association with a photon is measured in proton-proton collisions at a center-of-mass energy of 13 TeV. The data set, corresponding to an integrated luminosity of 137 fb^{-1} , was recorded by the CMS experiment during the 2016–2018 data taking of the LHC. The measurements are performed in a fiducial volume defined at the particle level. Events with an isolated, highly energetic lepton, at least three jets from the hadronization of quarks, among which at least one is b tagged, and one isolated photon are selected. The inclusive fiducial $t\bar{t}\gamma$ cross section, for a photon with transverse momentum greater than 20 GeV and pseudorapidity $|\eta| < 1.4442$, is measured to be 798 ± 7 (stat) ± 48 (syst) fb, in good agreement with the prediction from the standard model at next-to-leading order in quantum chromodynamics. The differential cross sections are also measured as a function of several kinematic observables and interpreted in the framework of the standard model effective field theory (EFT), leading to the most stringent direct limits to date on anomalous electromagnetic dipole moment interactions of the top quark and the photon.

Published in the Journal of High Energy Physics as doi:10.1007/JHEP12(2021)180.

1 Introduction

The large amount of proton-proton (pp) collision data at a center-of-mass energy of 13 TeV at the LHC allows for precision measurements of standard model (SM) processes with small production rates. Among these, top quark production provides a testing ground for the SM predictions and for phenomena beyond the SM (BSM). In particular, precise measurements of the inclusive and differential cross sections of top quark pair production in association with a high-energy photon ($t\bar{t}\gamma$) constrain anomalous $t\bar{t}\gamma$ electroweak interactions [1–4].

The CDF Collaboration at the Fermilab Tevatron measured the $t\bar{t}\gamma$ production cross section using proton-antiproton collisions at $\sqrt{s} = 1.96$ TeV [5], while at the LHC the measurement was performed in pp collisions at 7 TeV by the ATLAS [6], and at 8 TeV by both the ATLAS [7] and CMS [8] Collaborations. At 13 TeV, the ATLAS Collaboration measured inclusive and differential $t\bar{t}\gamma$ production cross sections in leptonic [9] and in the $e\mu$ [10] final states. All of these results are in agreement with the SM.

In this paper, the inclusive and differential $t\bar{t}\gamma$ production cross sections are measured in pp collisions at $\sqrt{s} = 13$ TeV. The analysis uses a data sample recorded with the CMS detector during Run 2 (2016–2018) of the LHC, which corresponds to an integrated luminosity of 137 fb^{-1} . The measurement is performed in the single-lepton (electron or muon) final state in a fiducial region defined at particle level. The inclusive fiducial $t\bar{t}\gamma$ cross section is measured for a selection on the photon transverse momentum of $p_T(\gamma) > 20 \text{ GeV}$ and the pseudorapidity of $|\eta(\gamma)| < 1.4442$, corresponding to the barrel region of the CMS electromagnetic calorimeter (ECAL). Differential cross sections are measured in the same fiducial region as a function of $p_T(\gamma)$, $|\eta(\gamma)|$, and the angular separation between the lepton and the photon, $\Delta R(\ell, \gamma)$. The observations are interpreted in the context of the SM effective field theory (SM-EFT) [11], where the c_{tZ} and c_{tZ}^{\perp} operators, defined in Ref. [12], are constrained using the measurement of the distribution of $p_T(\gamma)$. Tabulated results are provided in HEPDATA [13]. Examples of Feynman diagrams at leading order (LO) contributing to the $t\bar{t}\gamma$ signal topology are shown in Fig. 1.

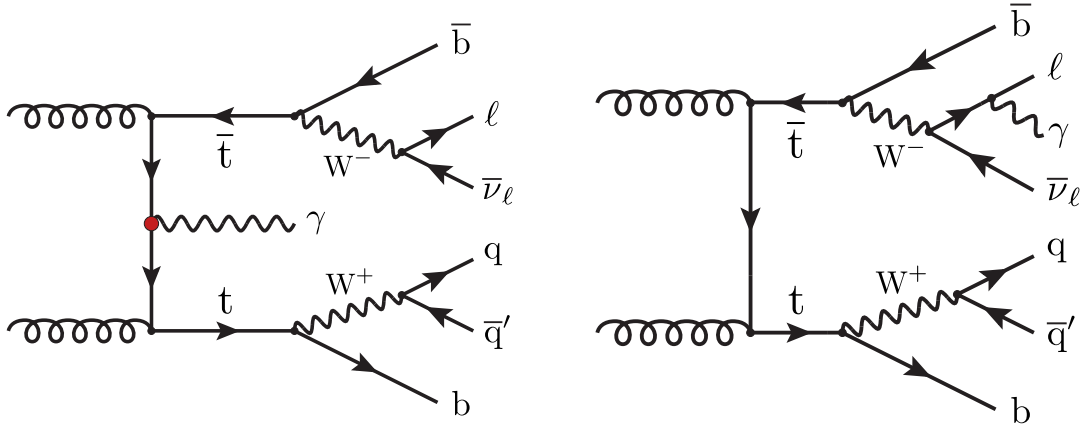


Figure 1: Representative LO Feynman diagrams for the $t\bar{t}\gamma$ signal process in the single-lepton channel, where the highly energetic photon originates from the top quark (left), or is emitted from a lepton (right). The $t\bar{t}\gamma$ interaction vertex is indicated by a circle.

This paper is organized as follows. The CMS detector is briefly introduced in Section 2. Details on the simulation of the signal and background processes and their modeling are provided in Section 3. The online selection, event reconstruction, and object definitions are described in Section 4. The fiducial phase space definition and photon categorization are described in Section 5. The event selection and the statistical treatment are discussed in Section 6. The procedures to estimate the backgrounds are described in Section 7 and the systematic uncertainties

are discussed in Section 8. The obtained results and the interpretation of the measurements in the context of SM-EFT are presented in Section 9. Finally, a summary is provided in Section 10.

2 The CMS detector

The central feature of the CMS apparatus is a superconducting solenoid of 6 m internal diameter, providing a magnetic field of 3.8 T. Within the solenoid volume are a silicon pixel and strip tracker, a lead tungsten crystal ECAL, and a brass and scintillator hadron calorimeter (HCAL), each composed of a barrel and two endcap sections. Forward calorimeters extend the η coverage provided by the barrel and endcap detectors that improve the measurement of the imbalance in transverse momentum. Muons are detected in gas-ionization chambers embedded in the steel flux-return yoke outside the solenoid.

Events of interest are selected using a two-tiered trigger system [14]. The first level trigger (L1) [15], composed of custom hardware processors, uses information from the calorimeters and muon detectors to select events at a rate of around 100 kHz within a fixed latency of about 4 μ s. The second level, known as the high-level trigger, consists of a farm of processors running a version of the full event reconstruction software optimized for fast processing, and reduces the event rate to around 1 kHz before data storage [14]. A more detailed description of the CMS detector, together with a definition of the coordinate system used and the relevant kinematic variables, can be found in Ref. [16].

3 Simulated event samples

Multiple Monte Carlo (MC) event generators are used to simulate the background and signal contributions, matching the varying conditions for each data-taking period. The $t\bar{t}$, t -channel single top quark, tW , and WW background processes are simulated at next-to-LO (NLO) in perturbative quantum chromodynamics (QCD) with the POWHEG v2 [17–23] event generator. The QCD multijet processes are generated with PYTHIA v8.226 (8.230) [24] for the 2016 (2017, 2018) data-taking period. All other background processes are simulated with MADGRAPH5_aMC@NLO v2.6.0 [25] at LO or NLO accuracy. The $t\bar{t}$ simulation is normalized to a cross section of 832 ± 42 pb calculated with the TOP++ v2.0 program [26] at next-to-NLO (NNLO), including resummation of next-to-next-to-leading-logarithm (NNLL) soft-gluon terms [27–32]. Events with an s - or t -channel produced top quark are normalized to NLO cross sections [33, 34], while the normalizations of WW and tW are at NNLO [35]. The overlap of the tW and $t\bar{t}$ simulation is removed using the diagram removal technique [36]. Drell–Yan and W +jets events are generated with up to four extra partons in the matrix element calculations with MADGRAPH5_aMC@NLO at LO and are normalized to NNLO cross sections [37–39] including electroweak corrections at NLO [40, 41]. The WZ , ZZ , $Z\gamma$, and $t\bar{t}W$ samples are simulated at NLO precision with one extra parton at ME level. The $W\gamma$ sample is simulated at LO precision with up to three extra partons. The $t\bar{t}Z$, $t\bar{t}W$, tZq , $t\gamma$, $W\gamma$, $Z\gamma$, and other diboson processes (WZ or ZZ) are normalized to the most precise cross sections available [42, 43].

The $t\bar{t}\gamma$ signal is generated with MADGRAPH5_aMC@NLO v2.6.0 at LO as a doubly resonant $2 \rightarrow 7$ process including all decay channels of the intermediate W bosons. It includes events where the photon is radiated from the intermediate top quarks, the intermediate W bosons and their decay products, the b quarks, and, in the case of quark-antiquark annihilation, radiation from initial-state quarks. The photon is required to satisfy $p_T > 10$ GeV and $|\eta| < 5$, while the lepton must pass $|\eta| < 5$. The angular separation ΔR between the photon and any of the seven final-state particles is required to be greater than 0.1, where $\Delta R = \sqrt{(\Delta\eta)^2 + (\Delta\phi)^2}$

Table 1: Event generator, perturbative order in QCD of the simulation, and perturbative order of the cross section normalization for each process.

Process	Event generator	Perturbative order of simulation	Cross section normalization
$t\bar{t}\gamma$	MADGRAPH5_aMC@NLO	LO	NLO
$t\bar{t}$	POWHEG	NLO	NNLO+NNLL [26–32]
Single t (t -channel)	POWHEG	NLO	NLO [33, 34]
Single t (s -channel)	MADGRAPH5_aMC@NLO	NLO	NLO [33, 34]
tW	POWHEG	NLO	NNLO [35]
Drell–Yan, W +jets	MADGRAPH5_aMC@NLO	LO	NNLO [37–41]
$W\gamma$	MADGRAPH5_aMC@NLO	LO	NLO
WW	POWHEG	NLO	NNLO [44]
$t\gamma, Z\gamma, WZ, ZZ$ $t\bar{t}Z, t\bar{t}W, tZq$	MADGRAPH5_aMC@NLO	NLO	NLO
Multijet	PYTHIA	LO	LO

and ϕ denotes the azimuthal angle. The renormalization scale (μ_R) and factorization scale (μ_F) are set to $\frac{1}{2} \sum_i \sqrt{m_i^2 + p_{T,i}^2}$, where the sum runs over all final-state particles generated at the matrix-element (ME) level. Although no photons are simulated at the ME level in the $t\bar{t}$ process, initial- and final-state photon radiation is accounted for in the showering algorithm. We remove double counting of the $t\bar{t}$ and $t\bar{t}\gamma$ samples by excluding events from the $t\bar{t}$ sample with a generated photon passing the photon requirements of the $t\bar{t}\gamma$ signal sample. The overlap between $W\gamma$ and W +jets, $Z\gamma$ and Drell–Yan, and $t\gamma$ and the single top quark t -channel process is removed analogously.

The event generators are interfaced with PYTHIA v8.226 (8.230) using the CP5 tune [45–47] for the 2016 (2017, 2018) samples to simulate multiparton interactions, fragmentation, parton shower, and hadronization of partons in the initial and final states, along with the underlying event. The NNPDF parton distribution functions (PDFs) v3.1 [48] are used according to the different perturbative order in QCD at the ME level. For the 2016 data-taking period, the CUETP8M1 tune [46] and the NNPDF PDFs v3.0 [49] are used for the Drell–Yan, W +jets, $t\gamma, Z\gamma, W\gamma$, diboson, $t\bar{t}W, t\bar{t}Z, tZq$, and multijet processes. Double counting of the partons generated with MADGRAPH5_aMC@NLO and PYTHIA is removed using the MLM [50] and the FxFx [51] matching schemes for LO and NLO samples, respectively. The events are subsequently processed with a GEANT4-based simulation model [52] of the CMS detector. All simulated samples include the effects of additional pp collisions in the same or adjacent bunch crossings (pileup), and are reweighted according to the observed distribution of the number of interactions in each bunch crossing [53]. In the following, to simplify the notation, the single top quark, $t\bar{t}$, and $t\gamma$ processes are grouped in the t/\bar{t} category, and furthermore, the $tZq, t\bar{t}W, t\bar{t}Z, WW, WZ,$ and ZZ processes in a category labeled “other”. A summary of the event samples is provided in Table 1.

4 Event reconstruction

Events are selected at the high-level trigger by the algorithms that require the presence of at least one lepton ($\ell = e$ or μ). The trigger threshold on the leading muon p_T is 27 (24) GeV in the 2017 (2016 and 2018) LHC running period. For electrons, the trigger threshold in the 2016 (2017–2018) period is 27 (32) GeV.

The particle-flow (PF) algorithm [54] aims to reconstruct and identify each individual particle in an event, with an optimized combination of information from the various elements of the CMS detector. The candidate vertex with the largest value of summed physics-object p_T^2 is taken to be the primary pp interaction vertex (PV). The energy of charged PF hadrons is determined from a combination of the track momentum and the matching ECAL and HCAL energy deposits, corrected for zero-suppression effects and for the response function of the calorimeters to hadronic showers. The energy of neutral PF hadrons is obtained from the corresponding corrected ECAL and HCAL energies.

The energy of electrons is determined from a combination of the electron momentum at the PV as determined by the tracker, the energy of the corresponding ECAL cluster, and the energy sum of all bremsstrahlung photons spatially compatible with originating from the electron track. Electron candidates are required to satisfy $p_T > 35$ GeV and $|\eta| < 2.4$, excluding the transition region between the barrel and endcap of the ECAL, $1.4442 < |\eta| < 1.5660$. The electron identification is performed using shower shape variables, track-cluster matching variables, and track quality variables. To reject electrons originating from photon conversion inside the detector, electrons are required to miss at most one possible hit in the innermost tracker layer and to be incompatible with any conversion-like secondary vertices.

The momentum of muons is obtained from the curvature of the corresponding track. Muon candidates are selected having $p_T > 30$ GeV and $|\eta| < 2.4$. The identification of muon candidates is performed using the quality of the geometrical matching between the measurements of the tracker and muon system [55].

The energy of photons is obtained from the ECAL measurement. Photon candidates are required to satisfy $p_T(\gamma) > 20$ GeV and to fall within the barrel of the ECAL, $|\eta| < 1.4442$. The identification of photons is based on isolation and shower shape information as a function of p_T and η , and takes into account pileup effects [56, 57]. In particular, the lateral shower extension must satisfy $\sigma_{\eta\eta}(\gamma) < 0.01$ for the chosen “medium” photon working point. It is defined as the second moment of a log-weighted distribution of crystal energies in η , calculated in the 5×5 matrix around the most energetic crystal in the photon’s supercluster [58]. Because of the reduced power of the $\sigma_{\eta\eta}(\gamma)$ observable in the ECAL endcap region in rejecting nonprompt photons, we find that excluding this $|\eta|$ range improves the uncertainties in the measurements.

All lepton and photon candidates are required to be isolated from other objects by selecting the reconstructed charged and neutral PF candidates in a cone around the candidate. A radius $\Delta R = 0.3$ (0.4) is used for electron (muon) candidates. For electron candidates, p_T - and η -dependent thresholds are set on the pileup corrected scalar p_T sum of photons and neutral and charged hadrons reconstructed by the PF algorithm ($I_{\text{rel}}(e)$) in the range of 5–10%. The chosen “tight” electron working point has a 70% efficiency while rejecting electron candidates originating from jets [58]. A muon candidate is isolated if it satisfies $I_{\text{rel}}(\mu) < 0.15$. The efficiency of the chosen “tight” working point is 90–95%, depending on p_T and η of the muon candidate [55]. For photon candidates, the scalar p_T sum of the charged particles within a cone of $\Delta R = 0.3$, denoted as the photon charged-hadron isolation, must satisfy $I_{\text{chg}}(\gamma) \leq 1.141$ GeV. Depending on the photon candidate p_T , there are separate requirements on the photon neutral-hadron and total isolation [58]. The photon reconstruction and selection efficiency for the chosen “medium” working point in simulation is on average 80%. The electron, muon, and photon reconstruction efficiencies are corrected as a function of the p_T and η of the reconstructed object to match the efficiency observed in data.

Furthermore, “loose” selection criteria are used to define control regions and to veto events with additional reconstructed leptons and photons. With respect to the tight electron selection,

the transverse momentum requirement is relaxed to $p_T > 15 \text{ GeV}$, the threshold on $I_{\text{rel}}(e)$ to the range of 20–25%, depending on p_T and η of the electron candidate, and two (three) missed hits in the innermost tracker layers are allowed for electrons in the barrel (endcap) region. The loose muon selection is based on Ref. [59] with $p_T > 15 \text{ GeV}$ and $I_{\text{rel}}(\mu) < 0.25$. The loose photon selection is defined by the “medium” photon working point without the $I_{\text{chg}}(\gamma)$ and $\sigma_{\eta\eta}(\gamma)$ requirements [58].

Jets are reconstructed by clustering PF candidates using the anti- k_T algorithm [60, 61] with a distance parameter of 0.4. Selected jets are required to satisfy $p_T > 30 \text{ GeV}$ and $|\eta| < 2.4$. Contributions to the clustered energy from pileup interactions are corrected for by requiring charged-hadron candidates to be associated with the PV and an offset correction for the contribution from neutral hadrons falling within the jet area is subtracted from the jet energy. Corrections to the jet energy scale (JES) are applied in simulation and data. The jet energy resolution (JER) is corrected in simulation to match the resolution observed in data [62].

Jets originating from the hadronization of b quarks are identified (b tagged) with a deep neural network algorithm [63] based on tracking and secondary vertex information. A working point is chosen such that the efficiency to identify the b jet is 55–70% for a jet p_T of 20–400 GeV. The misidentification rate in this p_T range is 1–2% for light-flavor and gluon jets, and up to 12% for charm quark jets. A correction is applied to the simulation to match the b tagging efficiencies observed in data.

The missing transverse momentum vector, \vec{p}_T^{miss} , is defined as the projection onto the plane perpendicular to the beams of the negative vector momentum sum of all PF candidates in an event. The JES and JER corrections are included in the \vec{p}_T^{miss} computation. Its magnitude is referred to as p_T^{miss} .

5 Fiducial phase space definition and photon classification

The fiducial region of the analysis is defined at the particle level by applying an event selection to the stable particles after the event generation, parton showering, and hadronization, but before the detector simulation.

Electrons (muons) must have $p_T > 35$ (30) GeV and $|\eta| < 2.4$, and must not originate from hadron decays. To account for final-state photon radiation, the four-momenta of photons inside a cone of $\Delta R = 0.1$ are added to the lepton before the lepton selection [64]. Events with leptonically decaying τ leptons in the decay chain of the top quark are considered signal.

Photons are selected if they do not originate from hadron decays, satisfy $p_T(\gamma) > 20 \text{ GeV}$ and $|\eta(\gamma)| < 1.4442$, and are found outside a cone of $\Delta R = 0.4$ around the leptons. An isolation requirement is applied by removing photons with stable particles (except neutrinos) found within a cone of $\Delta R = 0.1$ that satisfy $p_T > 5 \text{ GeV}$.

Particle-level jets are clustered using the anti- k_T algorithm with a distance parameter of 0.4, using all final-state particles, excluding neutrinos. Jets must satisfy $p_T > 30 \text{ GeV}$ and $|\eta| < 2.4$. A ghost matching method [65] is used to determine the flavor of the jets, with those matched to b hadrons tagged as b jets. Finally, the overlap of jets and other candidates is removed by excluding jets with $\Delta R \leq 0.4$ (0.1) to lepton (photon) candidates. A summary of the object definitions at particle level is provided in Table 2.

The fiducial region is constructed by requiring exactly one photon, exactly one lepton, and three or more jets among which at least one must be b tagged. The inclusive fiducial cross

Table 2: Overview of the definition of fiducial regions for various objects at particle level. A photon is isolated, if there are no stable particles (except neutrinos) with $p_T > 5$ GeV within a cone of $\Delta R = 0.1$.

Photon	e (μ)	Jet	b jet
$p_T > 20$ GeV	$p_T > 35$ (30) GeV	$p_T > 30$ GeV	$p_T > 30$ GeV
$ \eta < 1.4442$	$ \eta < 2.4$	$ \eta < 2.4$	$ \eta < 2.4$
no hadronic origin	no hadronic origin	$\Delta R(\text{jet}, \ell) > 0.4$	$\Delta R(\text{b jet}, \ell) > 0.4$
$\Delta R(\ell, \gamma) > 0.4$		$\Delta R(\text{jet}, \gamma) > 0.1$	$\Delta R(\text{b jet}, \gamma) > 0.1$
isolated			matched to b hadrons

section, predicted with MADGRAPH5_aMC@NLO at NLO in QCD, is 773 ± 135 fb. The NLO effects in the decay of the top quarks are not included in this calculation.

To facilitate the estimation of backgrounds with nonprompt and misidentified photons, a photon categorization is based on the matching between the reconstructed photon and simulated particles. Reconstructed photons are matched in ΔR to the corresponding generator-level particle from the primary interaction. The maximum ΔR considered for matching is 0.3 and the $p_T(\gamma)$ is required to be within 50% of the matched particle. Simulated events with a reconstructed photon are subsequently classified into three categories based on the matched generator particle. In the “genuine photon” category, the reconstructed photon is matched to a generated photon that originates from a lepton, a W boson, or a quark. In the “misidentified electron” category, the photon is matched to an electron. The “nonprompt photon” category is comprised of events where the photon is matched to a generated photon that originates from a hadron (71%), or in absence of a match to a generated photon or electron. This category thus includes contributions with misidentified photons and photons that originate from pileup interactions (29%).

6 Analysis strategy

6.1 Signal and control region definitions

The $t\bar{t}\gamma$ process typically produces events with several jets, up to two b-tagged jets, and an isolated photon with large p_T . The measurement is performed in signal regions with exactly one lepton ($N_\ell = 1$), exactly one photon ($N_\gamma = 1$), and at least three jets ($N_j \geq 3$), among which at least one is b tagged ($N_b \geq 1$). Events with additional leptons or photons passing the loose selection are removed. The measurement is performed in the $N_j = 3$ and ≥ 4 signal selections, denoted by SR3 and SR4p, respectively. Signal events with a jet failing the identification criteria thus enter the SR3 region. The $N_j \geq 3$ selection is denoted by SR3p. For illustration, Fig. 2 shows some kinematic distributions in the SR3p region where the simulated event samples are categorized according to the origin of the photon. The backgrounds are normalized according to the methods described in Sec. 7 and the pre-fit systematic uncertainties are shown as a hatched band. In this figure, M_3 denotes the invariant mass of the three-jet combination among all identified jets that maximizes the magnitude of the vector p_T sum [66]. This choice preferentially captures the hadronic top quark decay products.

The data-based estimation procedures for the dominant background sources are described in Sec. 7. The simulation predicts a significant background contribution from nonprompt photons (23%), misidentified electrons (19%), and a small contribution from multijet events in the SR3p region. The nonprompt photon contribution is estimated using background-enriched

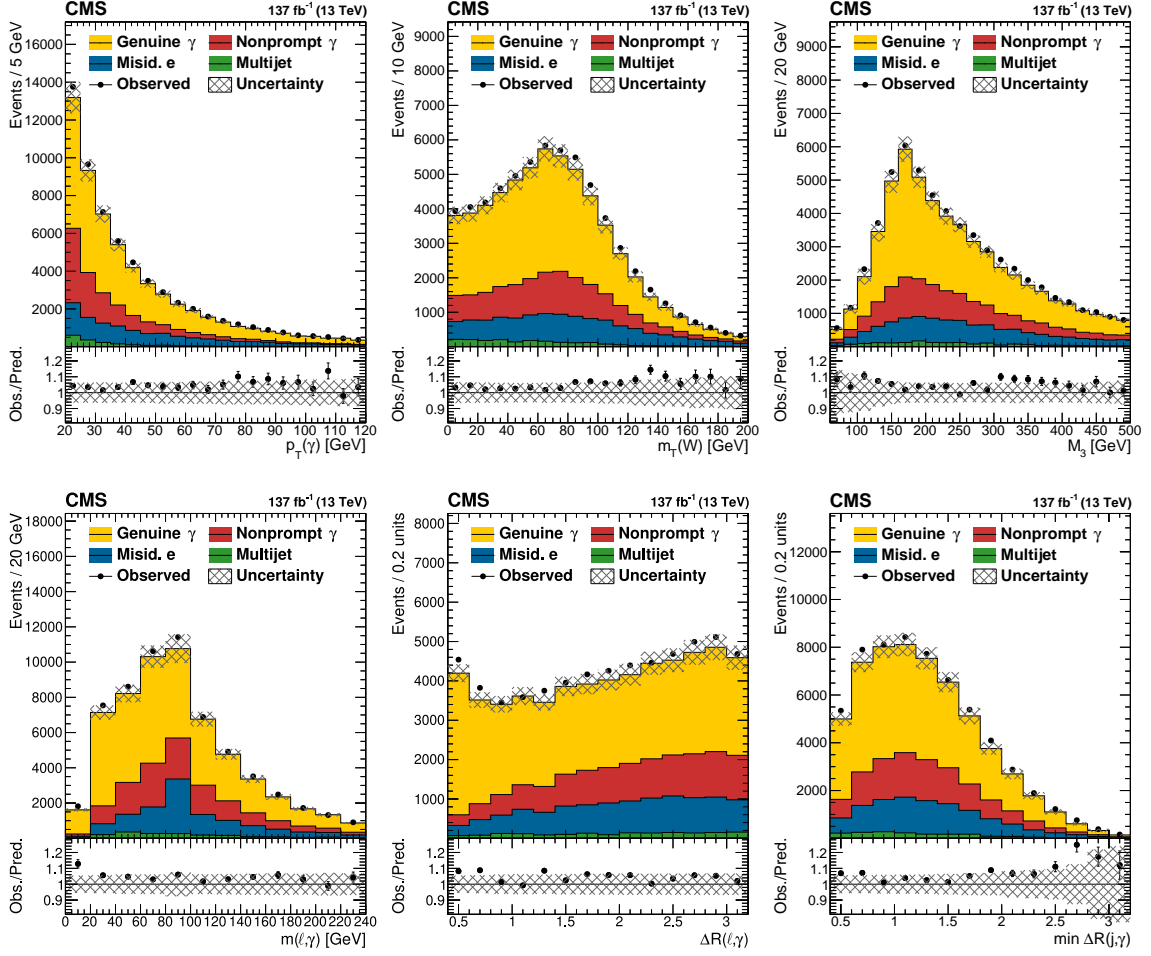


Figure 2: Distribution of $p_T(\gamma)$, the transverse mass $m_T(W)$ of the W boson candidate, the three-jet invariant mass M_3 (upper row); the invariant mass $m(\ell, \gamma)$ of the lepton and the photon, the angular separation $\Delta R(\ell, \gamma)$ of the lepton and the photon, and the minimal angular separation $\min \Delta R(j, \gamma)$ of the photon and all jets (lower row) in the SR3p region. The backgrounds are normalized according to the methods described in Sec. 7 and the pre-fit systematic uncertainties are shown as a hatched band. The lower panels show the ratio of the observed to the predicted event yields.

control regions with relaxed criteria on $I_{\text{chg}}(\gamma)$ and $\sigma_{\eta\eta}(\gamma)$. The multijet contributions to the signal and control regions are estimated by rescaling suitable normalized distributions (templates) obtained from background-enriched high- $I_{\text{rel}}(\ell)$ sidebands. The misidentified electron background is estimated in a $N_b = 0$ region where the invariant mass of the electron and photon candidates ($m(e, \gamma)$) is consistent with the Z boson hypothesis [67] within 10 GeV, i.e., $|m(e, \gamma) - m_Z| \leq 10 \text{ GeV}$, where m_Z is the Z boson mass. The control region is denoted by misDY3 (misDY4p) for $N_j = 3$ (≥ 4). The $W\gamma$ and the $Z\gamma$ processes contribute events with genuine photons to both the signal regions and the misDY3 and misDY4p control regions. In the electron channel, their contribution is constrained in “low mass” (LM) and “high mass” (HM) regions, defined by $m(e, \gamma) < m_Z - 10 \text{ GeV}$ and $m(e, \gamma) > m_Z + 10 \text{ GeV}$, respectively. In the muon channel, the LM (HM) region is defined by $m(\mu, \gamma) < m_Z$ ($m(\mu, \gamma) > m_Z$), where $m(\mu, \gamma)$ denotes the invariant mass of the muon and the photon. Table 3 provides a summary of the kinematic requirements in the signal and control regions.

Table 3: Overview of signal and control regions.

	Region	N_ℓ	N_j	N_b	N_γ	Other requirements
SR3p	SR3	1	3	≥ 1	1	
	SR4p	1	≥ 4	≥ 1	1	
LM3p	LM3	1	3	0	1	$m(e, \gamma) < m_Z - 10 \text{ GeV}$, $m(\mu, \gamma) < m_Z$
	LM4p	1	≥ 4	0	1	$m(e, \gamma) < m_Z - 10 \text{ GeV}$, $m(\mu, \gamma) < m_Z$
HM3p	HM3	1	3	0	1	$m(e, \gamma) > m_Z + 10 \text{ GeV}$, $m(\mu, \gamma) > m_Z$
	HM4p	1	≥ 4	0	1	$m(e, \gamma) > m_Z + 10 \text{ GeV}$, $m(\mu, \gamma) > m_Z$
misDY3p	misDY3	1	3	0	1	$ m(e, \gamma) - m_Z \leq 10 \text{ GeV}$
	misDY4p	1	≥ 4	0	1	$ m(e, \gamma) - m_Z \leq 10 \text{ GeV}$

6.2 Statistical treatment

The signal cross section is extracted from signal and control regions using the statistical procedure detailed in Refs. [68, 69]. The observed yields, signal and background estimates in each analysis category, and the systematic uncertainties are used to construct a binned likelihood function $L(r, \theta)$ as the product of Poisson probabilities of all bins. The nuisances related to the systematic uncertainties in the experiment and in the modeling of signal and background processes are described by log-normal probability density functions. The parameter r is the signal strength modifier, i.e., the ratio between the measured cross section and an arbitrary reference value of 773 fb, chosen as the nominal prediction for the inclusive fiducial cross section. The symbol θ represents the set of nuisance parameters describing the systematic uncertainties. The number of reconstructed $t\bar{t}\gamma$ signal events generated outside the fiducial phase space is scaled with the same value of r , i.e., no independent production cross section is assumed for this part of the signal.

The used test statistic is the profile likelihood ratio, $q(r) = -2 \ln L(r, \hat{\theta}_r) / L(\hat{r}, \hat{\theta})$, where $\hat{\theta}_r$ reflects the values of the nuisance parameters that maximize the likelihood function for a signal strength modifier r . The quantities \hat{r} and $\hat{\theta}$ are the values that simultaneously maximize L . A multi-dimensional fit is used to extract the observed cross section of the signal process, the nuisance parameters, and the uncertainties in the nuisance parameters [68, 69].

The LM3, LM4p, HM3, HM4p, misDY3 and misDY4p control regions enter the likelihood fit separately for each data-taking period and lepton flavor. In order to extract the $p_T(\gamma)$ dependence of the background with misidentified electrons, the misDY3 and misDY4p control regions are split into 7 bins separated by the $p_T(\gamma)$ thresholds 20, 35, 50, 65, 80, 120, and 160 GeV. The LM3, LM4p, HM3, and HM4p regions are similarly separated into 3 bins defined by the $p_T(\gamma)$ thresholds 20, 65, and 160 GeV. The binning is chosen to obtain a statistical uncertainty in simulated background yields of less than 15%.

The likelihood fit is performed for the inclusive cross section measurements, and separately for the differential measurement. For the extraction of the inclusive cross section, the SR3 and SR4p signal region are divided in three M_3 bins in the ranges 0–280, 280–420, and >420 GeV.

The binning in $p_T(\gamma)$, $|\eta(\gamma)|$, and $\Delta R(\ell, \gamma)$ in the SR3 and SR4p signal regions for the differential measurements is provided in Section 9.2. The estimation of contributions from various background processes is performed using control regions binned in $p_T(\gamma)$, which are used in all inclusive and differential measurements.

7 Background estimation

7.1 Multijet background

The probability for a multijet event to mimic the final state of the signal process is small and subject to large uncertainties. Therefore, the background from multijet events, comprising events with misidentified and nonprompt leptons, is estimated with a data-based procedure in sideband regions with loosened isolation criteria. For each N_j requirement, a sideband region is defined by $N_b = 0$ and requiring the lepton to pass the isolation criterion of the loose lepton working point and to fail the tight lepton selection. The $N_\gamma = 1$ requirement is kept. The resulting selection is dominated by multijet events. After electroweak backgrounds and backgrounds with top quarks (W +jets, $t/\bar{t}\bar{t}$, and Drell-Yan) are subtracted based on the expectation from simulation, templates for the distributions of kinematic observables are extracted.

The template normalization is evaluated from a transfer factor (“TF”), defined as the ratio of the multijet event yield with tightly isolated lepton candidates to the yield with loosely isolated lepton candidates. It is obtained in a selection with $N_j = 2$ and $N_\gamma = 0$ by fitting the distribution of the transverse mass of the W boson candidate, calculated from the formula

$$m_T(W) = \sqrt{2p_T^\ell p_T^{\text{miss}} [1 - \cos(\Delta\phi_{\ell, \vec{p}_T^{\text{miss}}})]} \quad (1)$$

where ℓ indicates the lepton considered in the event. The distribution is taken from data in a

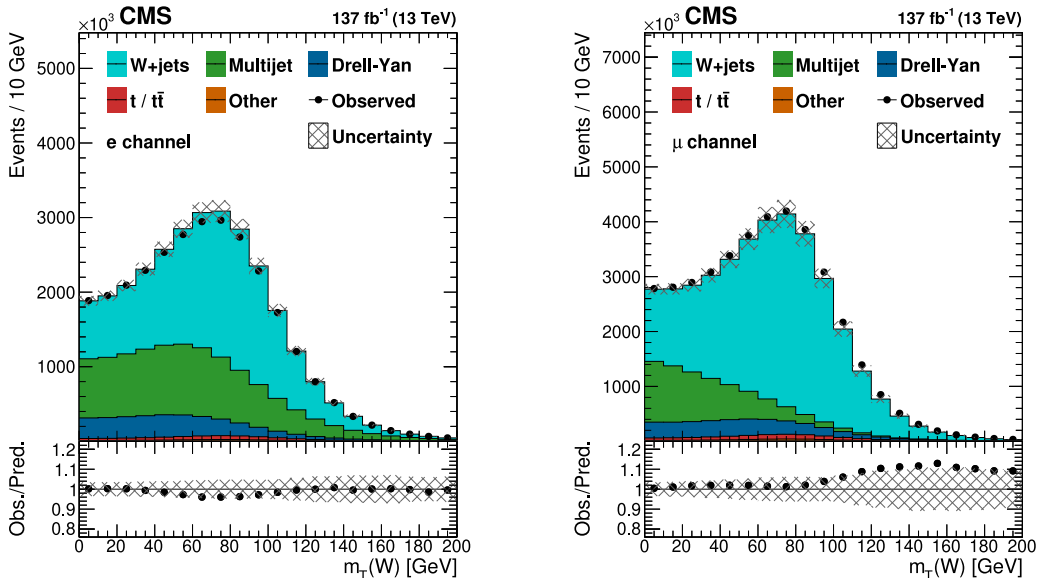


Figure 3: Fit result of the $m_T(W)$ multijet distribution in the selection with $N_j = 2$, $N_b = 0$, and tightly isolated electrons (left) and muons (right). The template obtained from the selection with loosely isolated leptons (green) and the total normalization of the electroweak and top quark background are floating in the fit. The lower panels show the ratio of the observed to the predicted event yields. The pre-fit systematic uncertainties are shown as a hatched band.

$N_b = 0$ selection with loosely isolated leptons, and electroweak and top quark backgrounds are subtracted. The fit is then performed in the selection with tightly isolated leptons where the total normalization of the electroweak and top quark background is left floating, while its shape is again taken from simulation. For illustration, the fit result for the $N_j = 2$ and $N_b = 0$ region, including the $m_T(W)$ multijet distribution from the selection with loosely isolated leptons, is shown in Fig. 3.

Because the efficiency of the tight lepton selection in multijet events depends on p_T and η of the lepton, the estimation procedure, including the TF fit, is performed in a total of 24 bins defined in these observables. Depending on p_T and η of the lepton, the TFs vary in the range of 0.9–3.1 (0.1–0.3) for the e channel and 2.0–3.7 (0.6–1.0) for the μ channel, for $N_b = 0$ (≥ 1). A correction based on simulated multijet events accounts for the TF dependence on N_j . Finally, the multijet estimate is obtained by scaling the $N_b = 0$ sideband templates with the corresponding TFs and accumulating the resulting predictions in the 24 bins in lepton p_T and η . The total multijet yield is estimated at 12 (8)% in the e (μ) channel in the LM3p, HM3p and misDY3p control regions and below 0.5% in the signal regions.

7.2 Nonprompt photon background

The nonprompt photon background component is estimated from data by exploiting the difference between its distribution in the plane defined by the weakly correlated variables $\sigma_{\eta\eta}(\gamma)$ with $I_{\text{chg}}(\gamma)$, and the corresponding distribution for genuine photons. In a sideband with a requirement of $\sigma_{\eta\eta}(\gamma) \geq 0.011$ on the photon candidate, the expected yields with genuine photons, misidentified electrons, and multijet events are subtracted. The sideband is used to obtain the normalization factor r_{SB} , defined as the ratio of the yield passing the $I_{\text{chg}}(\gamma) < 1.141$ GeV requirement to the event yield failing it. The estimation is obtained by multiplying r_{SB} with the yield in the normalization region, defined by the nominal $\sigma_{\eta\eta}(\gamma)$ requirement and the inverted criteria on the photon charged hadron isolation, $I_{\text{chg}}(\gamma) > 1.141$ GeV. The expected yields with genuine photons, misidentified electrons, and multijet events are subtracted from the observation in the normalization region. The procedure is carried out separately for lepton flavors, N_j selections, data-taking period, and for each bin of the differential cross section. The deviation from unity of the double-ratio of r_{SB} to the corresponding ratio in the nominal $\sigma_{\eta\eta}(\gamma)$ selection, stemming from the residual correlation between the two variables, is computed from simulation and it amounts to 18%. This value is used to correct the prediction.

7.3 Misidentified electron and genuine photon backgrounds

The background from electrons that are misidentified as photons is obtained from control regions defined by the requirements of $|m(e, \gamma) - m_Z| \leq 10$ GeV, and exactly three (misDY3), or four or more (misDY4p) jets. In the simulation, these event samples have a combined purity of 58% of Drell–Yan events with $Z \rightarrow ee$, where one of the electrons passes the photon selection criteria. The simulated yield of the background component with a misidentified electron is multiplied by the scale factor (SF) defined below, separately for each of the three data-taking periods.

The $W\gamma$ ($Z\gamma$) process contributes to the LM3p regions for both lepton flavors and has a purity of 41% (21%). In the HM3p regions, the $W\gamma$ background is dominant with a purity of 51%. The SFs for the misidentified electron background and the normalization of the $W\gamma$ and $Z\gamma$ processes are obtained from the likelihood fit as described in Section 6.2. The fit includes the data-based multijet estimates. The normalization of the $W\gamma$ process is left floating and the normalization of the $Z\gamma$ process is allowed to vary within its uncertainty. The resulting $m(\ell, \gamma)$ distributions are shown in Fig. 4 in the $N_j \geq 3$ control regions. The background with misidentified

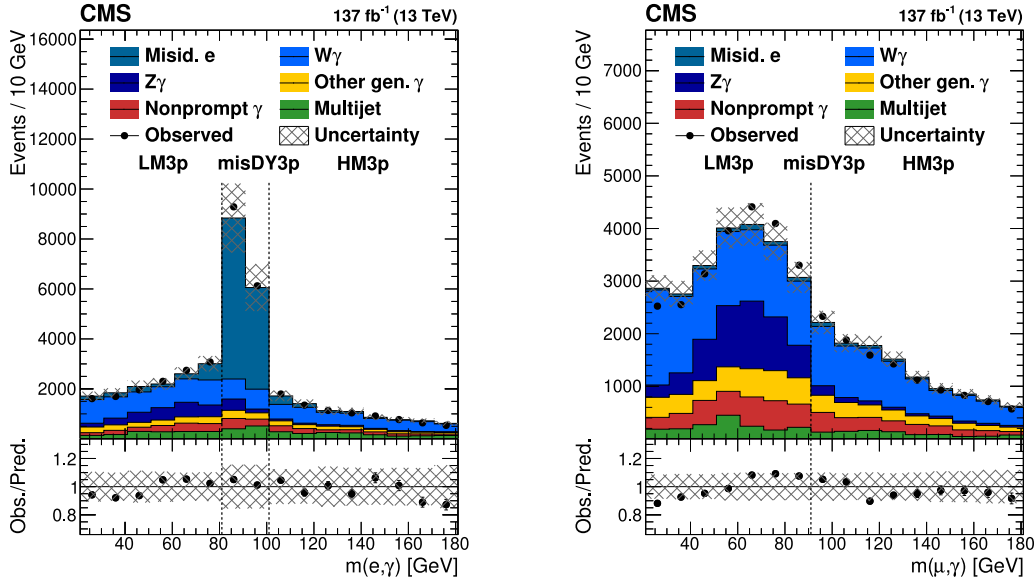


Figure 4: Distribution of the invariant mass of the lepton and the photon, $m(\ell, \gamma)$, in the $N_j \geq 3$, $N_b = 0$ selection for the e channel (left) and the μ channel (right). The genuine photon contributions of $W\gamma$ and $Z\gamma$ are visualized separately. The lower panels show the ratio of the observed to the predicted event yields. The pre-fit systematic uncertainties are shown as a hatched band.

electrons is dominant in the misDY3 and misDY4p regions close to the m_Z peak. A correction of 15% to the normalization of the Drell–Yan process is measured in a data sample with two well-identified leptons satisfying $|m(\ell, \ell) - m_Z| \leq 10$ GeV and $N_j \geq 3$, and is included in these results.

A summary of the extracted SF values for the misidentified electron background and the normalization of the $Z\gamma$ and $W\gamma$ processes, obtained from a profile likelihood fit excluding the signal regions, is provided in Table 4. The observed differences in the SFs for misidentified electrons are a result of the pixel detector replacement in 2017 and its operating conditions in the three data-taking periods. The stability of the procedure to estimate the yields of misidentified electrons and genuine photons is assessed by repeating the fit on individual data-taking periods and separately for the $N_j = 3$ and ≥ 4 selections. The extracted SFs from these checks agree within the uncertainties. For the measurements of the inclusive and differential cross sections, as well as for setting EFT limits, the SFs are determined in situ by performing the fit simultaneously with the signal regions.

Table 4: Extracted SFs and the total uncertainty obtained from the likelihood fit for the contribution from misidentified electrons for the three data-taking periods, and for the normalization of the $Z\gamma$ and $W\gamma$ background components.

Scale factor	Value
Misidentified electrons (2016)	2.25 ± 0.29
Misidentified electrons (2017)	2.00 ± 0.27
Misidentified electrons (2018)	1.52 ± 0.17
$Z\gamma$ normalization	1.01 ± 0.10
$W\gamma$ normalization	1.13 ± 0.08

8 Systematic uncertainties

The systematic uncertainties affecting the signal selection efficiency and background yields are summarized in Table 5. The table shows the range of variations in the different bins of the analysis caused by each systematic uncertainty in the signal and background yields, as well as an estimate of the impact of each uncertainty in the measured inclusive cross section. The table also indicates whether the uncertainties are treated as uncorrelated or fully correlated among the data-taking periods.

The integrated luminosities of the 2016, 2017, and 2018 data-taking periods are individually known with uncertainties in the 2.3–2.5% range [70–72], while the total Run 2 (2016–2018) integrated luminosity has an uncertainty of 1.8%, the improvement in precision reflecting the (uncorrelated) time evolution of some systematic effects. The uncertainty in the inclusive cross section from these sources is, therefore, 1.8%. Simulated events are reweighted according to the distribution of the number of interactions in each bunch crossing corresponding to a total inelastic pp cross section of 69.2 mb [53]. The uncertainty in the total inelastic pp cross section is 4.6% [73] and affects the pileup estimate. The uncertainty due to the pileup effect is about 2% for the expected yields and less than 0.5% for the inclusive cross section.

The uncertainties in the SFs used to match the simulated trigger selection efficiencies to the ones observed in data are propagated to the results. From the “tag-and-probe” measurement [56, 59], an uncertainty of up to 0.5% is assigned to the yields obtained in simulation. Lepton selection efficiencies are measured in bins of lepton p_T and η , and are found to be in the range 50–80 (75–85)% for electrons (muons). These measurements are performed separately in data and simulation and their ratio is used to scale the yields obtained in the simulation. The impact of these uncertainties on the inclusive cross section is 0.5 (0.7)% for the electron (muon) channel.

In the barrel section of the ECAL, an energy resolution of about 1% is achieved for unconverted or late-converting highly energetic photons in the tens of GeV energy range. The energy resolution of the remaining barrel photons is about 1.3% up to $|\eta| = 1$, changing to about 2.5% at $|\eta| = 1.4$ [57]. Uncertainties in the photon energy scale and resolution are measured with electrons from Z boson decays, reconstructed using information exclusively from the ECAL [57, 58]. Additionally, an event sample enriched in $\mu^+\mu^-\gamma$ events is used to measure an SF correcting the efficiency of the electron veto [74]. The total uncertainty in the photon energy and identification amounts to 1.1% for the inclusive cross section, and reaches 2% for $p_T(\gamma) > 100$ GeV.

The jet energy calibration accounts for the effects of pileup, the uniformity of the detector response, and residual data-simulation jet energy scale differences corrected using Drell–Yan, dijet, and γ +jet events. Uncertainties in the JES are estimated by shifting the jet energy corrections in simulation up and down by one standard deviation. Depending on p_T and η , the uncertainty in JES varies in the range 2–5%, leading to uncertainties in the predicted signal and background yields of 1.0–4.1% and an impact on the inclusive cross section of 1.9%. The dominant components originate from the uncertainty in the jet-flavor composition in the Drell–Yan and dijet selections (JES–FlavorQCD) and the absolute jet energy scale (JES–Absolute) [62]. For the signal and background processes modeled via simulation, the uncertainty in the measurement is determined from the observed differences in the yields with and without the shift in jet energy corrections. The same technique is used to calculate the uncertainties from the JER, which are found to be less than 1% [62]. The b tagging efficiency in the simulation is corrected using SFs determined from data, separately for b jets, c jets, and udsg jets [63, 75]. These are estimated separately for correctly and incorrectly identified jets, and each results in an uncertainty of about 0.8–1.6% in the yields in the signal regions, depending on N_b .

Table 5: Breakdown of the total uncertainty in its statistical and systematic components in the different signal regions. The first column indicates the source of the uncertainty. The second column shows the correlation between the data-taking periods. The third column shows the typical pre-fit uncertainties in the total simulated yields in the signal region. The last column gives the corresponding systematic uncertainty in the $t\bar{t}\gamma$ cross section from the fit to the data.

	Source	Correlation	Uncertainty [%]	
			yield	$\sigma(t\bar{t}\gamma)$
Experimental	Integrated luminosity	partial	2.3–2.5	1.8
	Pileup	100%	0.5–2.0	<0.5
	Trigger efficiency	—	<0.5	<0.5
	Electron reconstruction and identification	100%	0.2–1.7	<0.5
	Muon reconstruction and identification	partial	0.5–0.7	0.7
	Photon reconstruction and identification	100%	0.4–1.4	1.1
	$p_T(e)$ and $p_T(\gamma)$ reconstruction	100%	0.1–1.2	<0.5
	JES	partial	1.0–4.1	1.9
	JER	—	0.4–1.6	0.6
	b tagging	100% (2017/2018)	0.8–1.6	1.1
	L1 prefiring	100% (2016/2017)	0.3–0.9	<0.5
Theoretical	Tune	100%	0.1–1.9	<0.5
	Color reconnection	100%	0.4–3.6	<0.5
	ISR/FSR	100%	1.0–5.6	1.9
	PDF	100%	<0.5	<0.5
	ME scales μ_R, μ_F	100%	0.4–4.7	<0.5
Background	Multijet normalization	100%	1.3–6.5	0.9
	Nonprompt photon background	100%	1.2–2.7	1.8
	Misidentified e	—	2.5–8.0	1.8
	$Z\gamma$ normalization	100%	0.6–2.5	0.5
	$W\gamma$ normalization	100%	1.0–3.5	2.3
	DY normalization	100%	0.1–1.1	1.0
	$t/t\bar{t}$ normalization	100%	1.0–1.9	0.8
	$tW\gamma$ modeling	100%	1.6–4.4	1.6
	“Other” bkg. normalization	100%	0.3–1.0	<0.5
	Total systematic uncertainty			6.0
	Statistical uncertainty			0.9
	Total			6.0

During the 2016 and 2017 data-taking periods, a gradual shift in the timing of the inputs of the ECAL L1 trigger in the forward endcap region ($|\eta| > 2.4$) led to a specific inefficiency (labeled “L1 prefiring” in Table 5). A correction for this effect was determined using an unbiased data sample and is found to be relevant in events with jets with $2.4 < |\eta| < 3.0$ and $p_T > 100$ GeV. While no reconstructed objects at this η directly enter the measurements, it can affect the p_T^{miss} observable. A systematic variation of 20% of this correction for affected objects leads to an uncertainty of 0.3–0.9% in the predicted yields.

To estimate the theoretical uncertainties from missing higher-order corrections in the signal cross section calculation, the choice of μ_R and μ_F are varied independently up and down by a factor of 2. The acceptance variations are taken as the systematic uncertainty in each bin and are found to be smaller than 4.7%. Two independent nuisance parameters are used for the uncertainty in the choice of μ_R and μ_F , and their impact on the inclusive cross section measurement in the profile likelihood fit is less than 0.5%. A test with a single nuisance parameter, associated with the envelope of the uncertainties related to the choice of μ_R and μ_F , leads to negligible differences. The different sets in the NNPDF PDF [49] are used to estimate the corresponding uncertainty in the acceptance for the cross section measurement, which is less than 0.5%. The scale, PDF, and α_s uncertainties in the inclusive fiducial cross section of the $t\bar{t}\gamma$ process, evaluated with MADGRAPH5_aMC@NLO at NLO in QCD, amount to 17.5%. The limited number of available simulated events is considered by performing the fit using the Barlow–Beeston method [76].

In the parton shower simulation, the uncertainty from the choice of μ_F is estimated by varying the scale of initial- and final-state radiation (ISR/FSR) up and down by factors of 2 and $\sqrt{2}$, respectively, as suggested in Ref. [45]. The default configuration in PYTHIA includes a model of color reconnection based on multiple parton interactions (MPI) with early resonance decays switched off. To estimate the uncertainty from this choice of model, the variations of the simulated yields with different color reconnection schemes within PYTHIA are treated as systematic uncertainties: the MPI-based scheme with early resonance decays switched on, a gluon-move scheme [77], and a QCD-inspired scheme [78]. The total uncertainty from color reconnection modeling is estimated by taking the maximum deviation from the nominal result and amounts to less than 0.5% in the inclusive cross section.

The $tW\gamma$ background component amounts to at most 3.3% of the total event yield in the SR3 and SR4p signal regions and is predicted by the tW sample, simulated with POWHEG at NLO precision. To account for uncertainties in the $tW\gamma$ modeling, we treat the difference between the nominal prediction from the parton shower in the tW sample, normalized to NNLO, and a prediction obtained from MADGRAPH5_aMC@NLO at LO for the $2 \rightarrow 3$ process as an uncertainty. For the SR3 (SR4p) signal regions, the differences of the total $tW\gamma$ contribution are less than 44% (30%) in the $p_T(\gamma)$ bins, less than 34% (27%) in the $|\eta(\gamma)|$ bins, and less than 19% (17%) in the $\Delta R(\ell, \gamma)$ bins and lead to an uncertainty of 1.6% in the inclusive fiducial cross section.

The uncertainty in the normalization of the QCD multijet component is based on the variation of the TF with N_j for different N_b and amounts to 50%. Independent uncertainties are considered for the contributions to the $N_b = 0$ and ≥ 1 yields. These have a significant impact only in the LM3, LM4p, HM3, and HM4p control regions, and lead to an uncertainty of 0.9% in the measured inclusive cross section.

The uncertainty in the nonprompt photon prediction is based on the modeling of the $I_{\text{chg}}(\gamma)$ distribution for different requirements on $\sigma_{\eta\eta}(\gamma)$ and leads to an uncertainty of 1.8% in the inclusive cross section. The normalization of the $W\gamma$ process is left floating in the profile like-

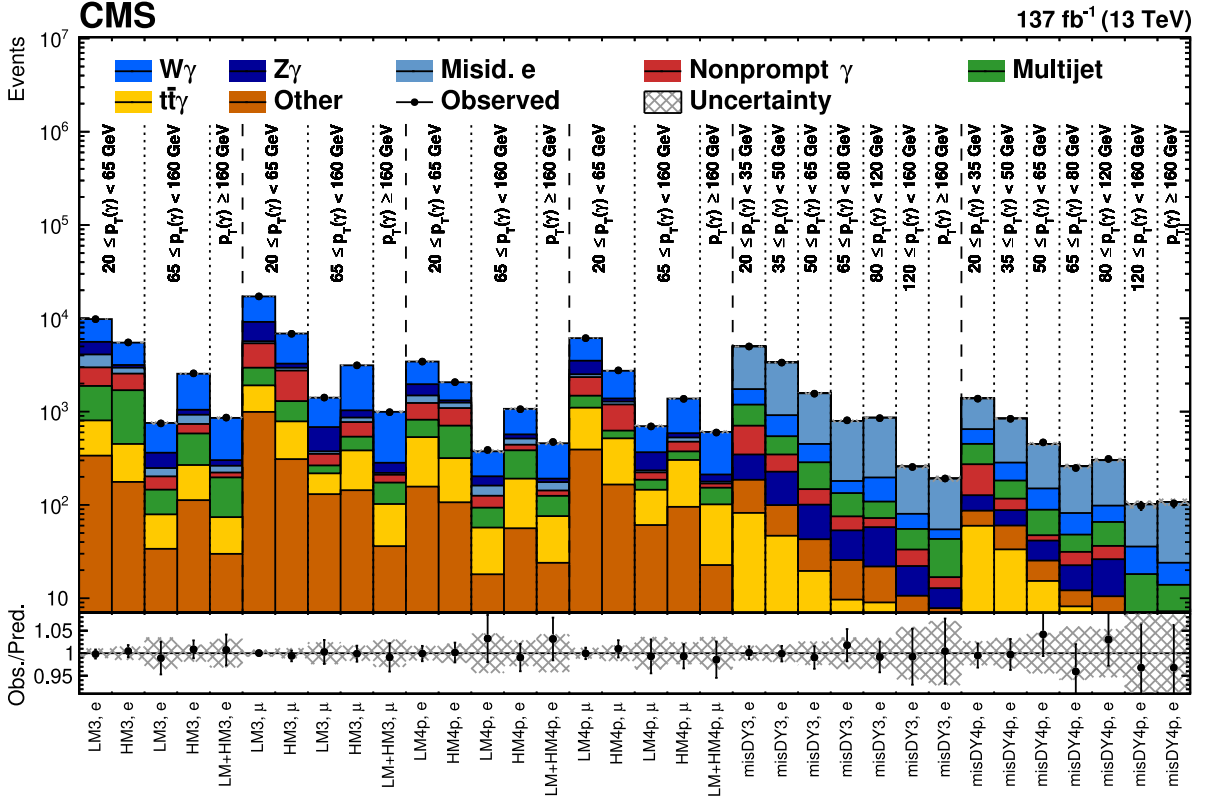


Figure 5: Fitted and observed yields in the LM3, LM4p, HM3, HM4p, misDY3, and misDY4p control regions using the post-fit values of the nuisance parameters. The lower panel shows the ratio of the observed to the predicted event yields. The post-fit systematic uncertainties are shown as a hatched band.

likelihood. To account for the uncertainty in the N_j modeling of the $Z\gamma$ process, we include an uncertainty of 30% in its normalization. In the signal region, the contribution of $W\gamma$ and $Z\gamma$ background events generated with additional b or c quarks is 30%, and we assign an uncertainty of 20% in its normalization. Moreover, 40 (20)% uncertainty is assigned to the normalization of the $Z\gamma$ ($W\gamma$ and misidentified electron) background in the $N_j \geq 4$ signal and control regions. The corresponding impact of the normalization of the $Z\gamma$ and $W\gamma$ contributions are 0.5 and 2.3%, respectively. The component with misidentified electrons leads to an uncertainty of up to 8% in the predicted background yields with an impact on the inclusive cross section of 1.8%. The 8% uncertainty in the normalization of the Drell–Yan process, the 5% uncertainty in the $t/t\bar{t}$ normalization, and the uncertainties in the normalization of other small background components lead to additional uncertainties below 1%.

9 Results

9.1 Inclusive cross section measurement

The observed data, as well as the predicted signal and background yields resulting from the likelihood fit to all signal and control regions, are shown in Figs. 5 and 6. In these figures, the contributions from the three data-taking periods are summed, accounting for the correlation of the systematic uncertainties. The signal cross section is extracted from these categories using the statistical procedure detailed in Section 6.2. In the fit, nuisance parameters for the various systematic uncertainties and the normalization of background processes, as described in

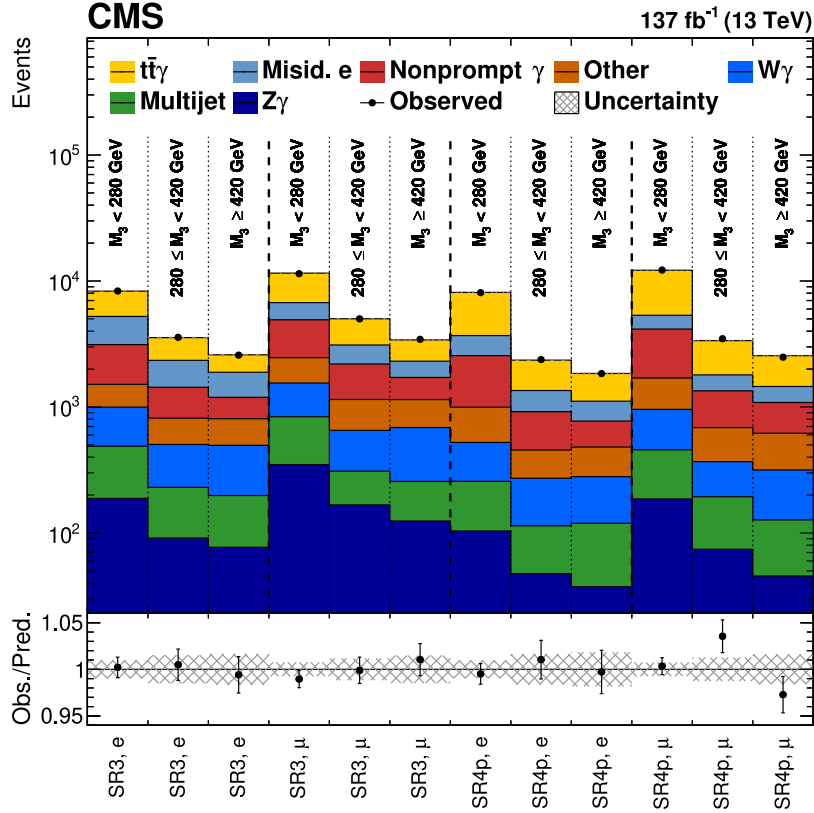


Figure 6: Fitted and observed yields in the SR3 and SR4p signal regions using the post-fit values of the nuisance parameters. The lower panel shows the ratio of the observed to the predicted event yields. The post-fit systematic uncertainties are shown as a hatched band.

Table 6: The observed number of events for the SR3 and SR4p signal regions in the e and μ channels, and the predicted yields and total post-fit uncertainties in each background component.

Process	SR3		SR4p	
	e	μ	e	μ
$t\bar{t}\gamma$	4995 ± 168	7821 ± 251	6174 ± 192	9495 ± 280
Misid. e	3710 ± 200	3322 ± 220	1904 ± 134	2015 ± 153
Nonprompt γ	2621 ± 107	4077 ± 161	2315 ± 124	3580 ± 149
Other	1136 ± 102	1866 ± 159	857 ± 110	1360 ± 166
$W\gamma$	1082 ± 77	1486 ± 108	585 ± 48	864 ± 74
Multijet	560 ± 104	762 ± 140	302 ± 65	472 ± 102
$Z\gamma$	356 ± 38	640 ± 68	189 ± 25	306 ± 40
Total	14459 ± 178	19976 ± 196	12326 ± 150	18093 ± 173
Observed	14479	19885	12305	18184

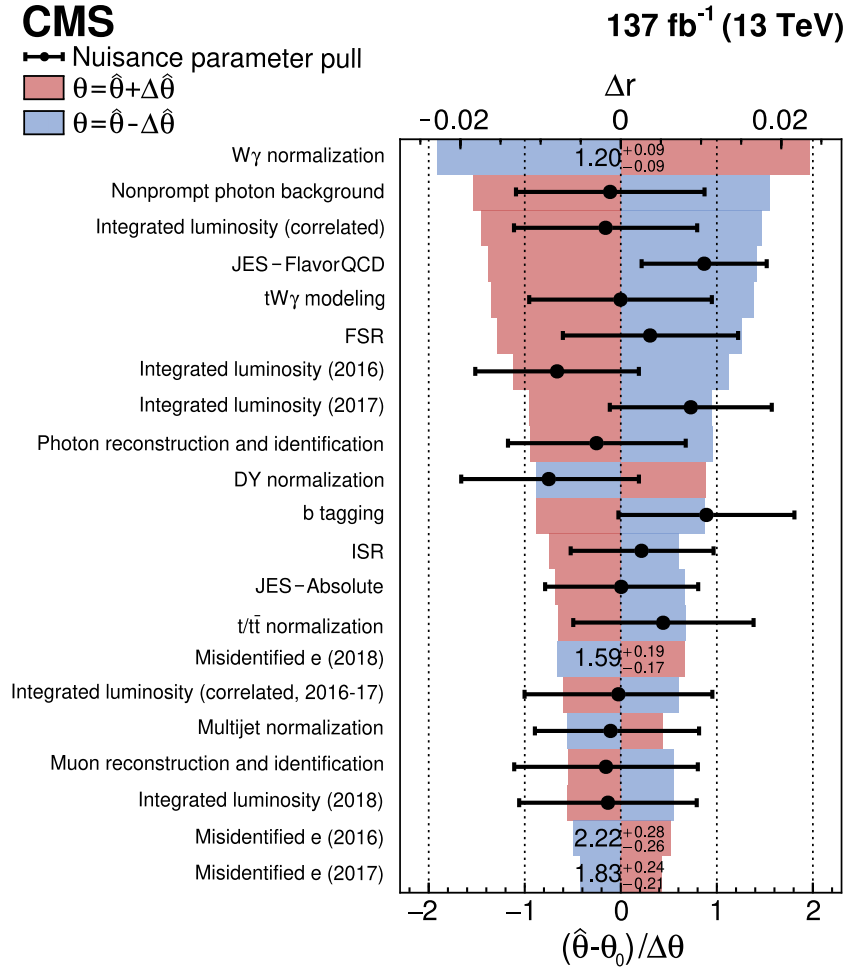


Figure 7: Ranking of the systematic uncertainties from the profile likelihood fit used in the inclusive cross section measurement. For each uncertainty, the red and blue bands indicate the post-fit impact on the fit result. The black dots indicate the post-fit values of the nuisance parameters and the numerical values provide the extracted SFs for the misidentified electron background and the normalization of the $W\gamma$ process. The black lines represent the post-fit uncertainties normalized to the pre-fit uncertainties (constraints).

Section 8, are included. The theoretical uncertainty in the inclusive fiducial cross section does not enter the likelihood fit for the inclusive or differential cross section measurements. Using three bins in M_3 reduces the uncertainty in the backgrounds without a hadronically decaying top quark, e.g., the misidentified electron background and the $W\gamma$ and $Z\gamma$ processes, and decreases the total relative uncertainty in the inclusive cross section from 6.7 to 6.0%. The observed number of events for the SR3 and SR4p signal regions in the e and μ channels, and the predicted yields and total uncertainties in each background component are listed in Table 6.

Figure 7 shows the ranking of the leading systematic uncertainties according to their post-fit impact on the measured inclusive cross section. The normalization of the $W\gamma$ background is the largest individual contribution to the uncertainty in the inclusive cross section measurement and amounts to about 2.3%. The post-fit values of the nuisance parameters (pulls) are also shown and are found to lie within the pre-fit uncertainties. The extracted SFs and the normalizations of the $Z\gamma$ and $W\gamma$ backgrounds also agree with the fit result in Table 4, obtained exclusively from the control regions. Besides the extraction of the nuisance parameters related

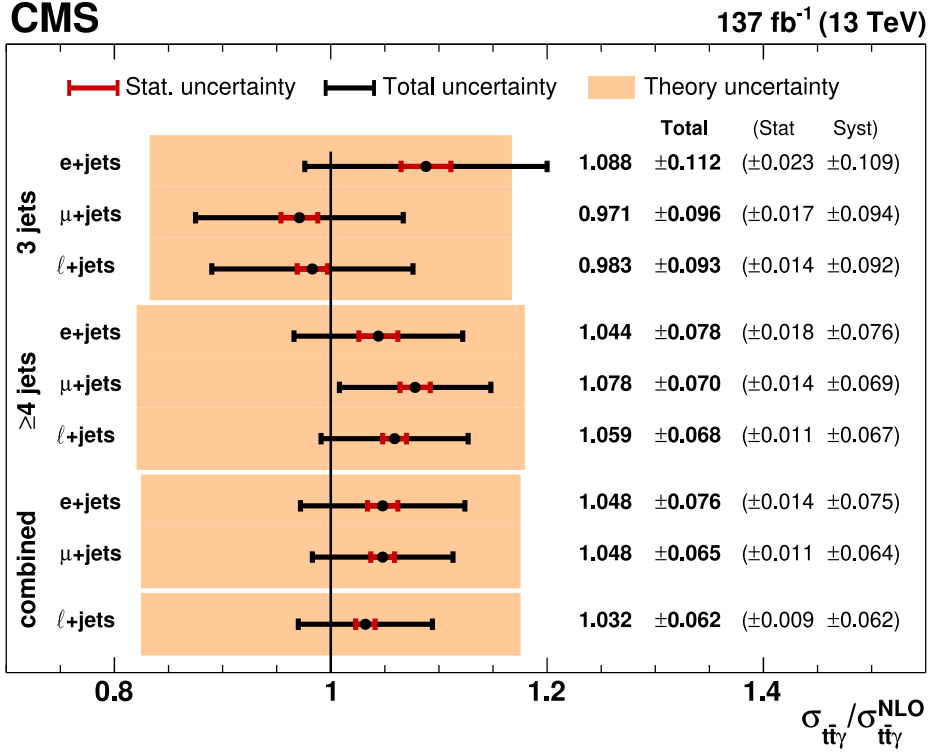


Figure 8: Summary of the measured cross section ratios with respect to the NLO cross section prediction for $N_j = 3, \geq 4$, and combined signal regions in the electron channel, muon channel, and the combined single-lepton channel. The orange band indicates the theory uncertainty in the prediction.

to the normalization of the misidentified electron component and the $Z\gamma$ and $W\gamma$ backgrounds, the only mild constraints are 35% for the JES–FlavorQCD nuisance and 25% for the scale of ISR. They reflect the improvement of the uncertainty in the inclusive cross section induced by the binning in M_3 .

The combined inclusive cross section of the $N_j = 3$ and ≥ 4 channels within the fiducial phase space is measured to be

$$\sigma(t\bar{t}\gamma) = 798 \pm 7 (\text{stat}) \pm 48 (\text{syst}) \text{ fb} \quad (2)$$

in good agreement with the SM expectation of $\sigma^{\text{NLO}}(t\bar{t}\gamma) = 773 \pm 135 \text{ fb}$. The measured value of the signal strength modifier is

$$r = 1.032 \pm 0.009 (\text{stat}) \pm 0.062 (\text{syst}). \quad (3)$$

A comparison of the measured cross sections and the SM prediction is shown in Fig. 8, providing also the measurements for different choices of N_j and the lepton flavor. For the latter results, the likelihood fit is performed separately in the corresponding set of signal regions and the full set of control regions.

9.2 Differential cross section measurement

The differential cross section is measured as a function of $p_T(\gamma)$, $|\eta(\gamma)|$, and $\Delta R(\ell, \gamma)$. Results are obtained simultaneously for the electron and muon channels, the 3 jet and ≥ 4 jet bins, and for the three data-taking periods. The binning in the SR3 and SR4p selections for the measurement of the differential distributions at the reconstruction level is shown in Table 7.

Table 7: Binning choices in the differential measurements at the reconstruction level.

$p_T(\gamma)$	20, 35, 50, 65, 80, 100, 120, 140, 160, 200, 260, ≥ 320 GeV
$ \eta(\gamma) $	0, 0.15, 0.30, 0.45, 0.60, 0.75, 0.90, 1.05, 1.20, 1.35, 1.4442
$\Delta R(\ell, \gamma)$	0.4, 0.6, 0.8, 1.0, 1.2, 1.4, 1.6, 1.8, 2.0, 2.2, 2.4, 2.6, 2.8, ≥ 3.0

As described in Section 6.2, the same control regions are used for the inclusive and differential cross section measurements. The signal strength is left floating in the profile likelihood fit separately for each of the differential bins, the N_j selection, the lepton flavor, and the data-taking period. The procedure has been tested to reproduce ad-hoc modifications of the simulated signal prediction within the numerical accuracy. The fit is performed separately for each differential distribution.

The distributions of the observables after background subtraction are further unfolded to the fiducial particle level phase space defined in Section 5. The unfolded differential cross section is defined in the same phase space as the inclusive cross section reported above, i.e., in the phase space where the top quark pair is produced in association with a photon satisfying $p_T(\gamma) > 20$ GeV and $|\eta(\gamma)| < 1.4442$. Signal events that are not generated within the fiducial region amount to 5–10% and are subtracted based on simulation. In the simulation, $p_T(\gamma)$ is taken as the transverse momentum after accounting for the effects of QCD and electroweak radiation.

The $t\bar{t}\gamma$ MADGRAPH5_aMC@NLO MC sample is used to construct a response matrix that takes into account both detector response and acceptance corrections. The same corrections, SFs, and uncertainties as used in the inclusive cross section are applied. Because of the high momentum- and angular resolutions of photons and leptons, the fraction of events migrating from a specific momentum region at the particle level to another one at the reconstruction level is small for all unfolded distributions. Under such conditions, and with the chosen bin size, no regularization term is required [79]. The TUNFOLD package [80] is used to obtain the results for the three measured observables using matrix inversion. The binning in the fiducial region is chosen such that two bins at the reconstruction level correspond to one bin in the fiducial region for most cases. This choice provides stability to the unfolding algorithm. The linearity of the unfolding procedure is tested by unfolding suitably reweighted simulated reconstruction-level yields. Differences between the unfolded reweighted distributions and the distributions resulting from the reweighting applied at the fiducial level are found to be negligible.

Uncertainties in the estimated signal yields are propagated through the unfolding procedure, including the effects on the response matrix. Experimental uncertainties from the detector response and efficiency, such as the photon identification, JES, and b tagging uncertainties, are applied as a function of the reconstructed observable. The differential cross sections, obtained by this procedure, are shown in Fig. 9. It includes a comparison with simulation obtained from MADGRAPH5_aMC@NLO interfaced to HERWIG++ [81] v2.7.1 with the EE5C tune [46] and to HERWIG7 v7.1.4 with the CH3 tune [82] for the parton shower and hadronization. The inclusive fiducial cross section predicted by HERWIG++ (HERWIG7) is 8.3% (5.4%) lower than for the nominal simulation.

The bin efficiency, defined as the fraction of generated events that are reconstructed in the corresponding bins at reconstruction level, is in the range of 20–30%. The bin purity, defined as the fraction of reconstructed events that originate from the corresponding bin at the particle level, is in the range of 85–90%. For $p_T(\gamma) > 120$ GeV, the uncertainties in the JES, the photon identification efficiency, and the color reconnection modeling are the largest sources of systematic uncertainty. The correlation matrices of the systematic uncertainties for the unfolded differen-

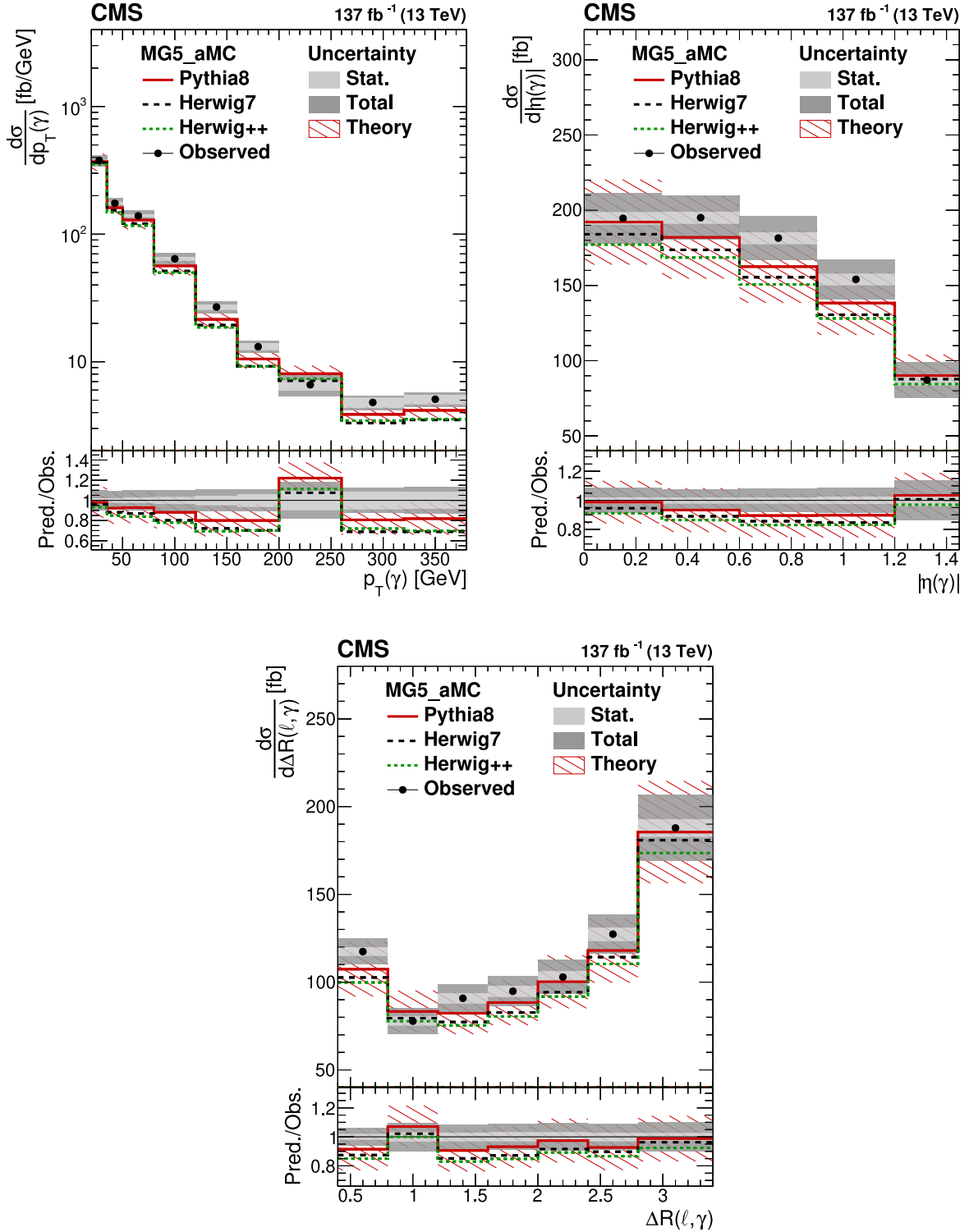


Figure 9: The unfolded differential cross sections for $p_T(\gamma)$ (upper left), $|\eta(\gamma)|$ (upper right), and $\Delta R(\ell, \gamma)$ (lower) compared with simulation obtained from the MADGRAPH5_aMC@NLO event generator interfaced to PYTHIA (red, solid), HERWIG7 (black, dashed) and HERWIG++ (green, dotted) for the parton shower and hadronization. For $p_T(\gamma)$ and $\Delta R(\ell, \gamma)$, the last bin includes the overflow. The lower panel displays the ratio of simulation to the observation. The inner and outer bands show the statistical and total uncertainties, respectively. Photons radiated from leptons and satisfying $\Delta R(\ell, \gamma) > 0.4$ are included in the signal and contribute significantly to the first bin of the differential $\Delta R(\ell, \gamma)$ cross section.

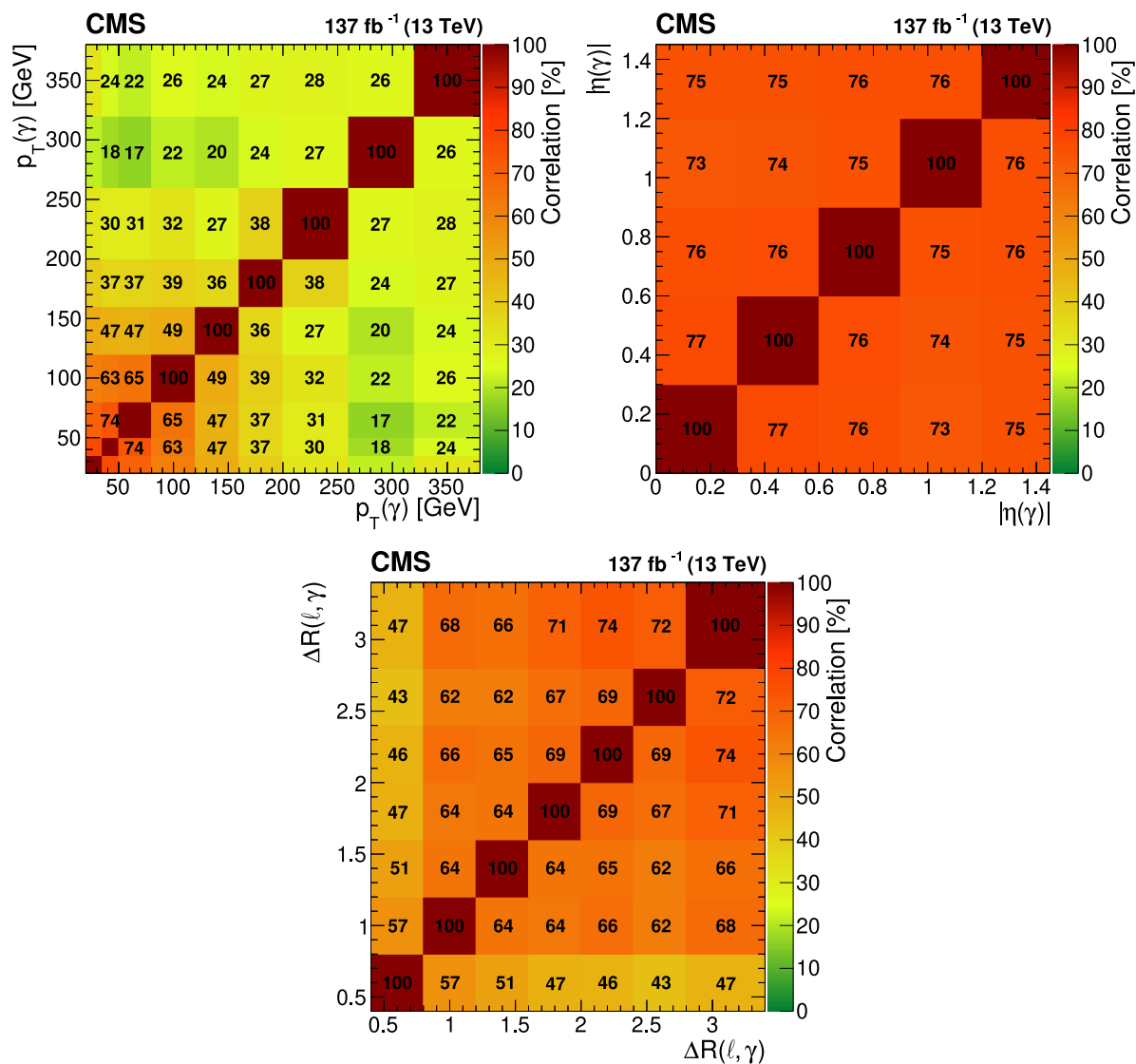


Figure 10: The correlation matrices of systematic uncertainties for the unfolded differential measurement for $p_T(\gamma)$ (upper left), $|\eta(\gamma)|$ (upper right), and $\Delta R(\ell, \gamma)$ (lower).

tial measurements are shown in Fig. 10. The correlations are lower in the tail of $p_T(\gamma)$ due to larger statistical uncertainties in the simulation. The first bin of the $\Delta R(\ell, \gamma)$ measurement is less affected by uncertainties in the normalization of backgrounds, resulting in slightly lower correlations in this case. All correlations from statistical uncertainties originating from the data are below 7%. Including the uncertainty in the fiducial signal cross section, we perform a compatibility test of the unfolded distribution and the nominal prediction. The corresponding χ^2 test statistic evaluates to 12.0 with 9 degrees of freedom (dof) for the $p_T(\gamma)$ distribution, 5.2 with 5 dof for $|\eta(\gamma)|$, and 6.3 with 7 dof for $\Delta R(\ell, \gamma)$.

9.3 Effective field theory interpretation

Many BSM models predict anomalous couplings of the top quark to the electroweak gauge bosons [83–89]. The differential cross section measurement is interpreted at the reconstruction level in SM-EFT in the Warsaw basis [90], formed by 59 baryon number conserving dimension-six Wilson coefficients. Among them, 15 are relevant for top quark interactions [91]. Anomalous interactions between the top quark and the gluon (chromomagnetic and chromoelectric dipole moment interactions) are tightly constrained by the $t\bar{t}$ +jets measurements [92, 93]. Similarly, the modification of the Wtb vertex is best constrained by measurements of the W helicity fractions in top quark pair production [94] and in t -channel single top quark production [95].

The Wilson coefficients in the Warsaw basis inducing electroweak dipole moments are denoted by $C_{uB}^{(33)}$ and $C_{uW}^{(33)}$ [12]. The SM gauge symmetry provides the $t\bar{t}Z$ and the $t\bar{t}\gamma$ final states with complementary constraining power [1–4]. The linear relations

$$\begin{aligned} c_{tZ} &= \text{Re} \left(-\sin \theta_W C_{uB}^{(33)} + \cos \theta_W C_{uW}^{(33)} \right), \\ c_{tZ}^I &= \text{Im} \left(-\sin \theta_W C_{uB}^{(33)} + \cos \theta_W C_{uW}^{(33)} \right), \\ c_{t\gamma} &= \text{Re} \left(\cos \theta_W C_{uB}^{(33)} + \sin \theta_W C_{uW}^{(33)} \right), \\ c_{t\gamma}^I &= \text{Im} \left(\cos \theta_W C_{uB}^{(33)} + \sin \theta_W C_{uW}^{(33)} \right), \end{aligned}$$

express the modifications of the $t\bar{t}Z$ interaction vertex, c_{tZ} and c_{tZ}^I , and of the $t\bar{t}\gamma$ interaction vertex, $c_{t\gamma}$ and $c_{t\gamma}^I$, in the Warsaw basis. The constraint $C_{uW}^{(33)} = 0$ ensures a SM Wtb vertex. Under this assumption, c_{tZ} (c_{tZ}^I) and $c_{t\gamma}$ ($c_{t\gamma}^I$) are dependent and we choose the former to parametrize the BSM hypothesis.

The spectrum of $p_T(\gamma)$ is a sensitive probe to such modifications. Other observables, e.g., $|\eta(\gamma)|$ or $\Delta R(\ell, \gamma)$, are found to be largely insensitive. Wilson coefficients that are not considered in this work are kept at their SM values and the SM-EFT expansion parameter is set to a mass scale $\Lambda = 1$ TeV. Using the SM-EFT parametrization from Ref. [12], simulated samples at the particle level are produced with nonzero values of the Wilson coefficients c_{tZ} and c_{tZ}^I . The $t\bar{t}\gamma$ signal process and all background processes affected by c_{tZ} or c_{tZ}^I at the ME level are included in the simulation. These samples are used to reweight the nominal simulation in the fiducial phase space using the quadratic parametrization detailed in Ref. [96]. The reweighting procedure is validated at the reconstruction level with a reduced set of statistically independent samples for nonzero values of c_{tZ} and c_{tZ}^I and excellent agreement is found.

The SR3 and SR4p signal regions and the $p_T(\gamma)$ boundaries defining the bins in Table 7 are used to construct a binned likelihood function $L(\theta)$ as a product of Poisson probabilities from the yields in the signal and control regions. The nuisance parameters are labeled by θ and the

profile likelihood ratio $q = -2\ln(L(\hat{\theta}, \vec{C})/L(\hat{\theta}_{\max}))$ is the test statistic. Here, $\hat{\theta}$ is the set of nuisance parameters maximizing the likelihood function at a BSM point defined by the Wilson coefficients collectively denoted by \vec{C} . In the denominator, $\hat{\theta}_{\max}$ maximizes the likelihood function in the BSM parameter space. The $t\bar{t}\gamma$ signal is normalized according to the SM expectation at NLO in QCD and its uncertainty is included as a nuisance.

Figure 11 shows the result of the fit for the SR3 and SR4p signal regions and separately for each lepton flavor. No deviations from the SM expectations are observed. The best fit point is found at $(c_{tZ}, c_{tZ}^I) = (-0.28, -0.02)$ and the corresponding spectrum is overlaid together with the ones from several other choices for nonzero values of the Wilson coefficients. Figure 12 displays the one-dimensional scans of the coefficients. In the upper row, one Wilson coefficient is scanned, while the other is profiled. The lower row shows the scans, where the second Wilson coefficient is set to zero. The second local minima in the scans of the log-likelihood as a function of c_{tZ} and c_{tZ}^I , visible in Fig. 12 (lower row), is the result of a mild tension with the SM hypothesis in conjunction with the similarity of the predictions for Wilson coefficients with opposite sign. The corresponding one-dimensional intervals at 68 and 95% confidence interval (CL) are listed in Table 8 and are more stringent than previous limits obtained from $t\bar{t}Z$ final states [97, 98]. Models with nonzero electroweak dipole moments predict a harder $p_T(\gamma)$ spectrum that is not observed in data. Figure 13 shows the best fit result in the two-dimensional plane spanned by c_{tZ} and c_{tZ}^I and the log-likelihood scan. The SM prediction is within the 95% CL of the best fit value of the c_{tZ} and c_{tZ}^I coefficients.

In Fig.14, the 95% CL intervals are compared with the previous CMS results based on the inclusive [99] and differential [97] $t\bar{t}Z$ cross section measurement, a CMS result based on $t\bar{t}$ in final states with additional leptons [96], and the most recent ATLAS result [98] (lower). The result of a global SM-EFT analysis, including results from Ref. [97], is also shown [100]. The present result improves upon the previous constraints by about a factor of 2.5.

Table 8: Summary of the one-dimensional intervals at 68 and 95% CL.

		Wilson coefficient	68% CL interval (Λ/TeV) ²	95% CL interval (Λ/TeV) ²
Expected	c_{tZ}	$c_{tZ}^I = 0$	[-0.19, 0.20]	[-0.29, 0.31]
		profiled	[-0.19, 0.20]	[-0.29, 0.31]
	c_{tZ}^I	$c_{tZ} = 0$	[-0.20, 0.20]	[-0.30, 0.30]
		profiled	[-0.20, 0.20]	[-0.30, 0.30]
Observed	c_{tZ}	$c_{tZ}^I = 0$	[-0.36, -0.17]	[-0.43, 0.38]
		profiled	[-0.36, 0.04]	[-0.43, 0.38]
	c_{tZ}^I	$c_{tZ} = 0$	[-0.36, -0.16], [0.18, 0.35]	[-0.43, 0.43]
		profiled	[-0.32, 0.31]	[-0.42, 0.42]

10 Summary

A measurement of the cross section for the top quark pair production in association with a photon using a data sample of proton-proton collisions at $\sqrt{s} = 13\text{ TeV}$, corresponding to an integrated luminosity of 137 fb^{-1} , collected with the CMS detector at the LHC has been

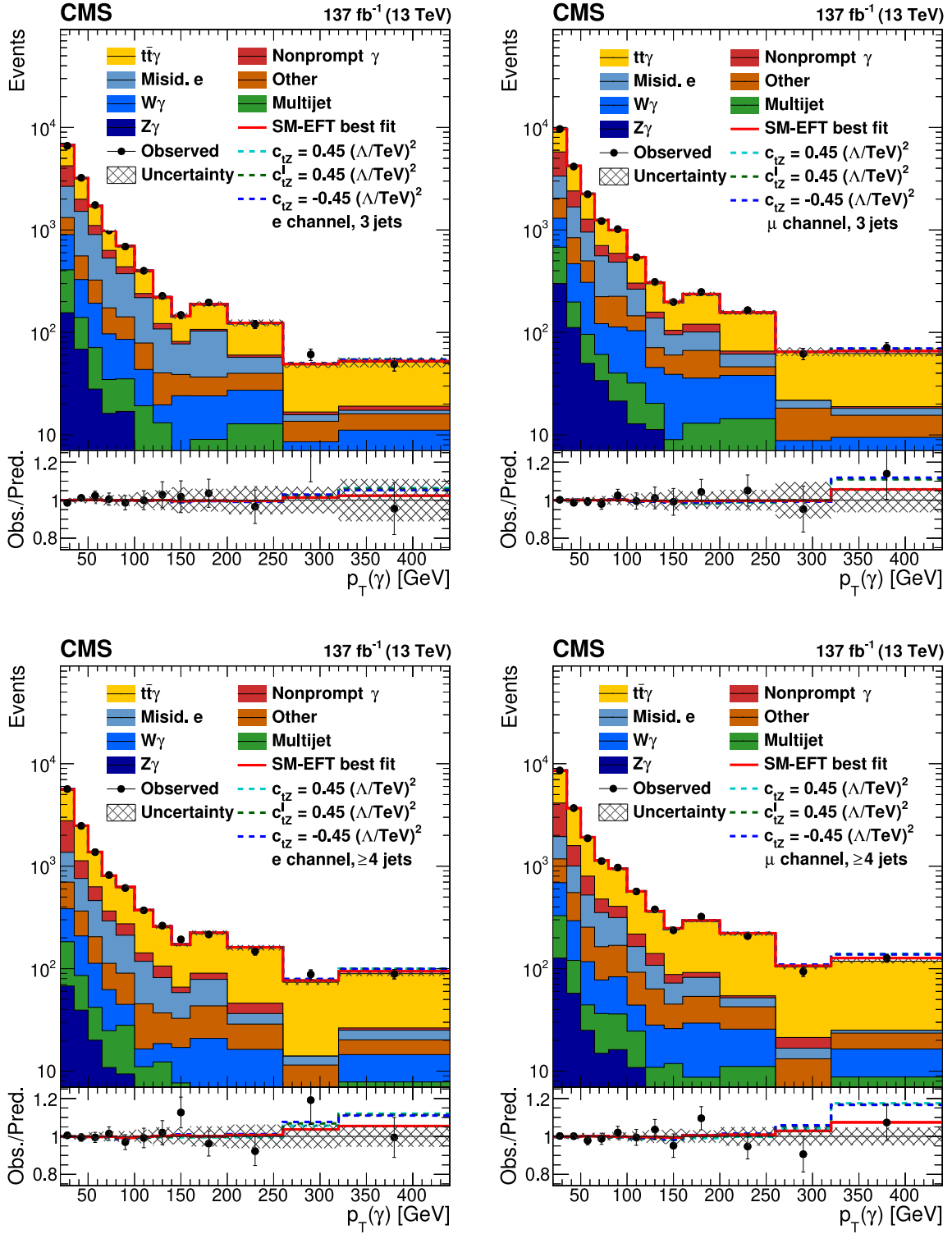


Figure 11: The observed (points) and predicted (shaded histograms) post-fit yields for the combined Run 2 data set in the SR3 (upper) and SR4p (lower) signal regions for the electron (left) and muon channel (right). The vertical bars on the points give the statistical uncertainties in the data. The lower panel displays the ratio of the data to the predictions and the hatched regions show the total uncertainty. The solid line shows the SM-EFT best fit prediction and the dashed lines show different predictions for nonzero Wilson coefficients, $c_{tZ} = 0.45$ (light blue), $c_{tZ}^1 = 0.45$ (green), and $c_{tZ} = -0.45$ (dark blue), where Λ is set to 1 TeV.

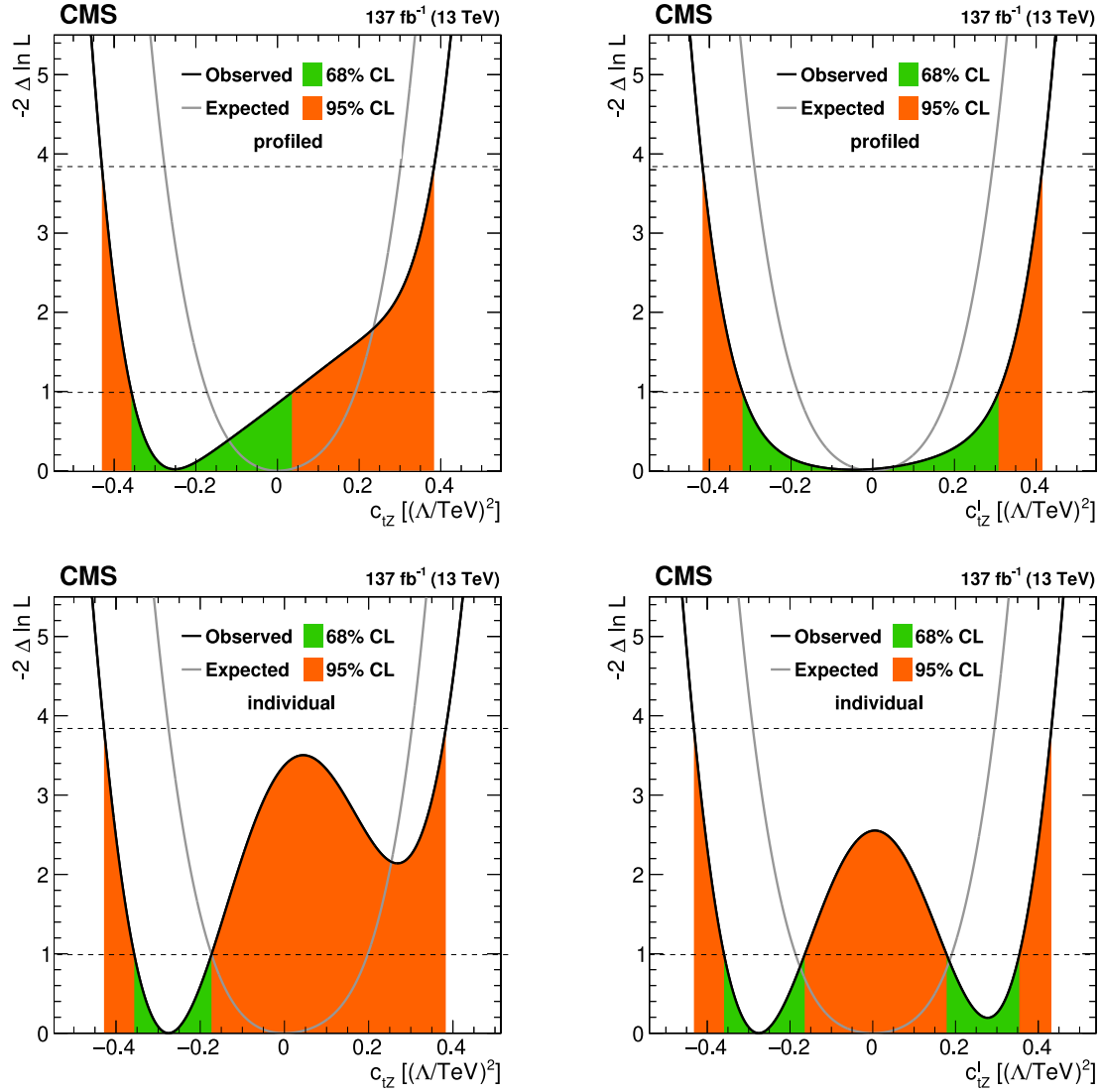


Figure 12: Results of the one-dimensional scans of the Wilson coefficients c_{tZ} (left) and c_{tZ}^1 (right). In the upper row, the other Wilson coefficient is profiled, while in the lower row it is set to zero. The green and orange bands indicate the 68 and 95% CL contours on the Wilson coefficients, respectively.

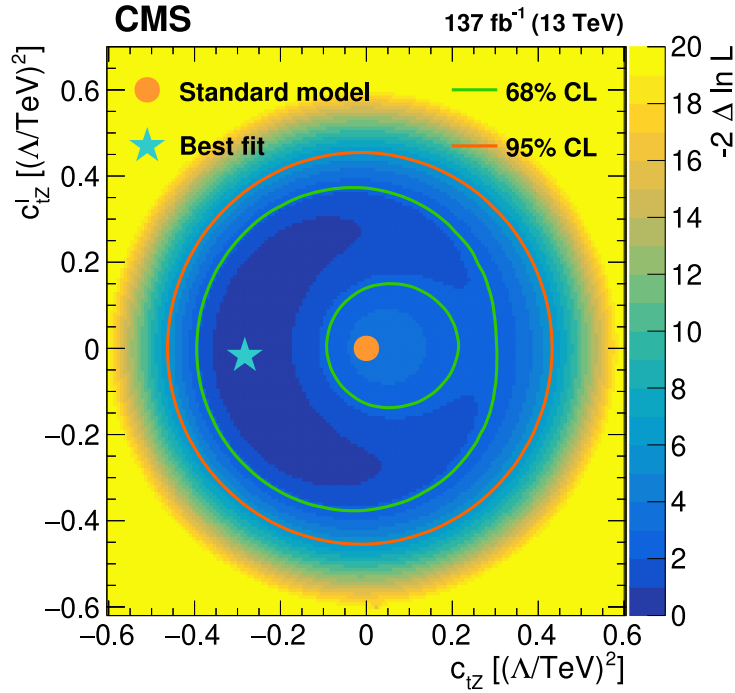


Figure 13: Result of the two-dimensional scan of the Wilson coefficients c_{tZ} and c_{tZ}^1 . The shading quantified by the color scale on the right reflects the negative log-likelihood ratio with respect to the best fit value that is designated by the star. The green and orange lines indicate the 68 and 95% CL contours from the fit, respectively. The allowed areas are those between the two green contours and that inside the orange contour. The dot shows the SM prediction.

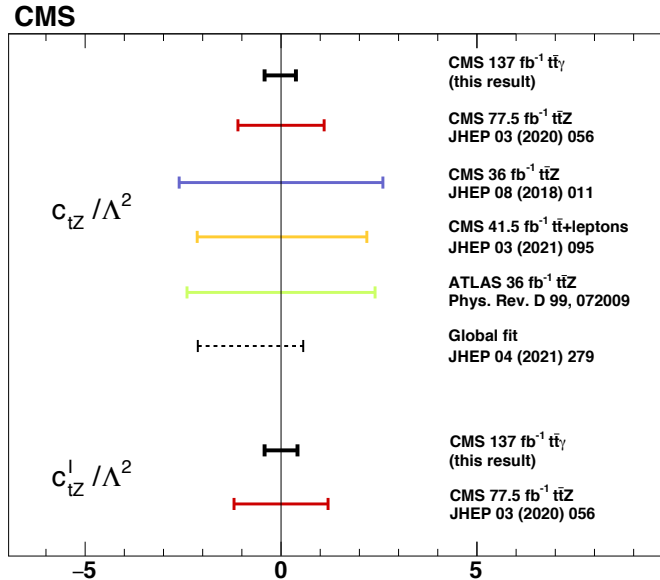


Figure 14: The observed 95% CL intervals for the Wilson coefficients from this measurement with the other Wilson coefficient set to zero, the previous CMS results based on the inclusive [99] and differential [97] $t\bar{t}Z$ cross section measurement, a CMS result based on $t\bar{t}$ in final states with additional leptons [96], and the most recent ATLAS result [98]. The result of a global SM-EFT analysis, including results from Ref. [97], is also shown [100]. The vertical line displays the SM prediction.

presented. It is the first result of the CMS Collaboration on measurements in the $t\bar{t}\gamma$ final state using 13 TeV data. The analysis has been performed in the single-lepton channel with events with exactly three and four or more jets among which at least one is b tagged. Background components with misidentified electrons, photons originating in the hadronization of jets, the multijet component, and prompt photons from the $W\gamma$ and $Z\gamma$ processes are estimated from data. The measured inclusive cross section in a fiducial region with photon transverse momentum $p_T(\gamma) > 20$ GeV and jet multiplicity greater than three is measured to be 798 ± 7 (stat) ± 48 (syst) fb, in good agreement with the standard model prediction at next-to-leading order in quantum chromodynamics.

Differential cross sections for $p_T(\gamma)$ and absolute value of the photon pseudorapidity, as well as for the angular separation of the lepton and the photon, have been measured and unfolded to particle level in the same fiducial volume. The comparison to simulation was performed using different showering algorithms. The measurements are also interpreted in terms of limits on the Wilson coefficients in the context of the standard model effective field theory. The confidence intervals for the Wilson coefficients c_{tZ} and c_{tZ}^I are the most stringent to date.

Acknowledgments

We congratulate our colleagues in the CERN accelerator departments for the excellent performance of the LHC and thank the technical and administrative staffs at CERN and at other CMS institutes for their contributions to the success of the CMS effort. In addition, we gratefully acknowledge the computing centers and personnel of the Worldwide LHC Computing Grid and other centers for delivering so effectively the computing infrastructure essential to our analyses. Finally, we acknowledge the enduring support for the construction and operation of the LHC, the CMS detector, and the supporting computing infrastructure provided by the following funding agencies: BMBWF and FWF (Austria); FNRS and FWO (Belgium); CNPq, CAPES, FAPERJ, FAPERGS, and FAPESP (Brazil); MES (Bulgaria); CERN; CAS, MoST, and NSFC (China); MINCIENCIAS (Colombia); MSES and CSF (Croatia); RIF (Cyprus); SENESCYT (Ecuador); MoER, ERC PUT and ERDF (Estonia); Academy of Finland, MEC, and HIP (Finland); CEA and CNRS/IN2P3 (France); BMBF, DFG, and HGF (Germany); GSRT (Greece); NKFI (Hungary); DAE and DST (India); IPM (Iran); SFI (Ireland); INFN (Italy); MSIP and NRF (Republic of Korea); MES (Latvia); LAS (Lithuania); MOE and UM (Malaysia); BUAP, CINVESTAV, CONACYT, LNS, SEP, and UASLP-FAI (Mexico); MOS (Montenegro); MBIE (New Zealand); PAEC (Pakistan); MSHE and NSC (Poland); FCT (Portugal); JINR (Dubna); MON, RosAtom, RAS, RFBR, and NRC KI (Russia); MESTD (Serbia); SEIDI, CPAN, PCTI, and FEDER (Spain); MOSTR (Sri Lanka); Swiss Funding Agencies (Switzerland); MST (Taipei); ThEPCenter, IPST, STAR, and NSTDA (Thailand); TUBITAK and TAEK (Turkey); NASU (Ukraine); STFC (United Kingdom); DOE and NSF (USA).

Individuals have received support from the Marie-Curie program and the European Research Council and Horizon 2020 Grant, contract Nos. 675440, 724704, 752730, 765710 and 824093 (European Union); the Leventis Foundation; the Alfred P. Sloan Foundation; the Alexander von Humboldt Foundation; the Belgian Federal Science Policy Office; the Fonds pour la Formation à la Recherche dans l'Industrie et dans l'Agriculture (FRIA-Belgium); the Agentschap voor Innovatie door Wetenschap en Technologie (IWT-Belgium); the F.R.S.-FNRS and FWO (Belgium) under the "Excellence of Science – EOS" – be.h project n. 30820817; the Beijing Municipal Science & Technology Commission, No. Z191100007219010; the Ministry of Education, Youth and Sports (MEYS) of the Czech Republic; the Deutsche Forschungsgemeinschaft (DFG), under Germany's Excellence Strategy – EXC 2121 "Quantum Universe" – 390833306, and under project number 400140256 - GRK2497; the Lendület ("Momentum") Program and the János Bolyai Research Scholarship of the Hungarian Academy of Sciences, the New National Excellence Program ÚNKP, the NKFI research grants 123842, 123959, 124845, 124850, 125105, 128713, 128786, and 129058 (Hungary); the Council of Science and Industrial Research, India; the Latvian Council of Science; the Ministry of Science and Higher Education and the National Science Center, contracts Opus 2014/15/B/ST2/03998 and 2015/19/B/ST2/02861 (Poland); the National Priorities Research Program by Qatar National Research Fund; the Ministry of Science and Higher Education, project no. 0723-2020-0041 (Russia); the Programa Estatal de Fomento de la Investigación Científica y Técnica de Excelencia María de Maeztu, grant MDM-2015-0509 and the Programa Severo Ochoa del Principado de Asturias; the Thalís and Aristeia programs cofinanced by EU-ESF and the Greek NSRF; the Rachadapisek Sompot Fund for Postdoctoral Fellowship, Chulalongkorn University and the Chulalongkorn Academic into Its 2nd Century Project Advancement Project (Thailand); the Kavli Foundation; the Nvidia Corporation; the SuperMicro Corporation; the Welch Foundation, contract C-1845; and the Weston Havens Foundation (USA).

References

- [1] U. Baur, A. Juste, L. H. Orr, and D. Rainwater, “Probing electroweak top quark couplings at hadron colliders”, *Phys. Rev. D* **71** (2005) 054013, doi:10.1103/PhysRevD.71.054013, arXiv:hep-ph/0412021.
- [2] A. O. Bouzas and F. Larios, “Electromagnetic dipole moments of the top quark”, *Phys. Rev. D* **87** (2013) 074015, doi:10.1103/PhysRevD.87.074015, arXiv:1212.6575.
- [3] M. Schulze and Y. Soreq, “Pinning down electroweak dipole operators of the top quark”, *Eur. Phys. J. C* **76** (2016) 466, doi:10.1140/epjc/s10052-016-4263-x, arXiv:1603.08911.
- [4] R. Röntsch and M. Schulze, “Probing top-Z dipole moments at the LHC and ILC”, *JHEP* **08** (2015) 044, doi:10.1007/JHEP08(2015)044, arXiv:1501.05939.
- [5] CDF Collaboration, “Evidence for $t\bar{t}\gamma$ production and measurement of $\sigma_{t\bar{t}\gamma}/\sigma_{t\bar{t}}$ ”, *Phys. Rev. D* **48** (2011) 031104, doi:10.1103/PhysRevD.84.031104, arXiv:1106.3970.
- [6] ATLAS Collaboration, “Observation of top-quark pair production in association with a photon and measurement of the $t\bar{t}\gamma$ production cross section in pp collisions at $\sqrt{s} = 7$ TeV using the ATLAS detector”, *Phys. Rev. D* **91** (2015) 072007, doi:10.1103/PhysRevD.91.072007, arXiv:1502.00586.
- [7] ATLAS Collaboration, “Measurement of the $t\bar{t}\gamma$ production cross section in proton-proton collisions at $\sqrt{s} = 8$ TeV with the ATLAS detector”, *JHEP* **11** (2017) 086, doi:10.1007/JHEP11(2017)086, arXiv:1706.03046.
- [8] CMS Collaboration, “Measurement of the semileptonic $t\bar{t}+\gamma$ production cross section in pp collisions at $\sqrt{s} = 8$ TeV”, *JHEP* **10** (2017) 006, doi:10.1007/JHEP10(2017)006, arXiv:1706.08128.
- [9] ATLAS Collaboration, “Measurements of inclusive and differential fiducial cross-sections of $t\bar{t}\gamma$ production in leptonic final states at $\sqrt{s} = 13$ TeV in ATLAS”, *Eur. Phys. J. C* **79** (2019) 382, doi:10.1140/epjc/s10052-019-6849-6, arXiv:1812.01697.
- [10] ATLAS Collaboration, “Measurements of inclusive and differential cross-sections of combined $t\bar{t}\gamma$ and $tW\gamma$ production in the $e\mu$ channel at 13 TeV with the ATLAS detector”, *JHEP* **09** (2020) 049, doi:10.1007/JHEP09(2020)049, arXiv:2007.06946.
- [11] O. Bessidskaia Bylund et al., “Probing top quark neutral couplings in the standard model effective field theory at NLO in QCD”, *JHEP* **05** (2016) 052, doi:10.1007/JHEP05(2016)052, arXiv:1601.08193.
- [12] D. Barducci et al., “Interpreting top-quark LHC measurements in the standard-model effective field theory”, 2018. arXiv:1802.07237.
- [13] “HEPData record for this analysis”, 2021. doi:10.17182/hepdata.102876.
- [14] CMS Collaboration, “The CMS trigger system”, *JINST* **12** (2017) P01020, doi:10.1088/1748-0221/12/01/P01020, arXiv:1609.02366.

-
- [15] CMS Collaboration, “Performance of the CMS Level-1 trigger in proton-proton collisions at $\sqrt{s} = 13$ TeV”, *JINST* **15** (2020) P10017, doi:10.1088/1748-0221/15/10/P10017, arXiv:2006.10165.
- [16] CMS Collaboration, “The CMS experiment at the CERN LHC”, *JINST* **3** (2008) S08004, doi:10.1088/1748-0221/3/08/S08004.
- [17] P. Nason, “A new method for combining NLO QCD with shower Monte Carlo algorithms”, *JHEP* **11** (2004) 040, doi:10.1088/1126-6708/2004/11/040, arXiv:hep-ph/0409146.
- [18] S. Frixione, P. Nason, and C. Oleari, “Matching NLO QCD computations with parton shower simulations: the POWHEG method”, *JHEP* **11** (2007) 070, doi:10.1088/1126-6708/2007/11/070, arXiv:0709.2092.
- [19] S. Alioli, P. Nason, C. Oleari, and E. Re, “A general framework for implementing NLO calculations in shower Monte Carlo programs: the POWHEG BOX”, *JHEP* **06** (2010) 043, doi:10.1007/JHEP06(2010)043, arXiv:1002.2581.
- [20] J. M. Campbell, R. K. Ellis, P. Nason, and E. Re, “Top-pair production and decay at NLO matched with parton showers”, *JHEP* **04** (2015) 114, doi:10.1007/JHEP04(2015)114, arXiv:1412.1828.
- [21] S. Alioli, P. Nason, C. Oleari, and E. Re, “NLO single-top production matched with shower in POWHEG: s - and t -channel contributions”, *JHEP* **09** (2009) 111, doi:10.1088/1126-6708/2009/09/111, arXiv:0907.4076. [Erratum: doi:10.1007/JHEP02(2010)011].
- [22] S. Frixione, P. Nason, and G. Ridolfi, “A positive-weight next-to-leading-order Monte Carlo for heavy flavour hadroproduction”, *JHEP* **09** (2007) 126, doi:10.1088/1126-6708/2007/09/126, arXiv:0707.3088.
- [23] E. Re, “Single-top Wt -channel production matched with parton showers using the POWHEG method”, *Eur. Phys. J. C* **71** (2011) 1547, doi:10.1140/epjc/s10052-011-1547-z, arXiv:1009.2450.
- [24] T. Sjöstrand et al., “An introduction to PYTHIA 8.2”, *Comput. Phys. Commun.* **191** (2015) 159, doi:10.1016/j.cpc.2015.01.024, arXiv:1410.3012.
- [25] J. Alwall et al., “The automated computation of tree-level and next-to-leading order differential cross sections, and their matching to parton shower simulations”, *JHEP* **07** (2014) 079, doi:10.1007/JHEP07(2014)079, arXiv:1405.0301.
- [26] M. Czakon and A. Mitov, “Top++: a program for the calculation of the top-pair cross-section at hadron colliders”, *Comput. Phys. Commun.* **185** (2014) 2930, doi:10.1016/j.cpc.2014.06.021, arXiv:1112.5675.
- [27] M. Beneke, P. Falgari, S. Klein, and C. Schwinn, “Hadronic top-quark pair production with NNLL threshold resummation”, *Nucl. Phys. B* **855** (2012) 695, doi:10.1016/j.nuclphysb.2011.10.021, arXiv:1109.1536.
- [28] M. Cacciari et al., “Top-pair production at hadron colliders with next-to-next-to-leading logarithmic soft-gluon resummation”, *Phys. Lett. B* **710** (2012) 612, doi:10.1016/j.physletb.2012.03.013, arXiv:1111.5869.

- [29] P. Bärnreuther, M. Czakon, and A. Mitov, “Percent level precision physics at the Tevatron: First genuine NNLO QCD corrections to $q\bar{q} \rightarrow t\bar{t}+X$ ”, *Phys. Rev. Lett.* **109** (2012) 132001, doi:10.1103/PhysRevLett.109.132001, arXiv:1204.5201.
- [30] M. Czakon and A. Mitov, “NNLO corrections to top-pair production at hadron colliders: the all-fermionic scattering channels”, *JHEP* **12** (2012) 054, doi:10.1007/JHEP12(2012)054, arXiv:1207.0236.
- [31] M. Czakon and A. Mitov, “NNLO corrections to top pair production at hadron colliders: the quark-gluon reaction”, *JHEP* **01** (2013) 080, doi:10.1007/JHEP01(2013)080, arXiv:1210.6832.
- [32] M. Czakon, P. Fiedler, and A. Mitov, “Total top-quark pair-production cross section at hadron colliders through $O(\alpha_s^4)$ ”, *Phys. Rev. Lett.* **110** (2013) 252004, doi:10.1103/PhysRevLett.110.252004, arXiv:1303.6254.
- [33] M. Aliev et al., “HATHOR: HAdronic Top and Heavy quarks crOss section calculatoR”, *Comput. Phys. Commun.* **182** (2011) 1034, doi:10.1016/j.cpc.2010.12.040, arXiv:1007.1327.
- [34] P. Kant et al., “HATHOR for single top-quark production: Updated predictions and uncertainty estimates for single top-quark production in hadronic collisions”, *Comput. Phys. Commun.* **191** (2015) 74, doi:10.1016/j.cpc.2015.02.001, arXiv:1406.4403.
- [35] N. Kidonakis, “Theoretical results for electroweak-boson and single-top production”, *PoS DIS2015* (2015) 170, doi:10.22323/1.247.0170, arXiv:1506.04072.
- [36] S. Frixione et al., “Single-top hadroproduction in association with a W boson”, *JHEP* **07** (2008) 029, doi:10.1088/1126-6708/2008/07/029, arXiv:0805.3067.
- [37] K. Melnikov and F. Petriello, “Electroweak gauge boson production at hadron colliders through $O(\alpha_s^2)$ ”, *Phys. Rev. D* **74** (2006) 114017, doi:10.1103/PhysRevD.74.114017, arXiv:hep-ph/0609070.
- [38] S. Catani et al., “Vector boson production at hadron colliders: a fully exclusive QCD calculation at NNLO”, *Phys. Rev. Lett.* **103** (2009) 082001, doi:10.1103/PhysRevLett.103.082001, arXiv:0903.2120.
- [39] C. Anastasiou, L. J. Dixon, K. Melnikov, and F. Petriello, “High precision QCD at hadron colliders: Electroweak gauge boson rapidity distributions at NNLO”, *Phys. Rev. D* **69** (2004) 094008, doi:10.1103/PhysRevD.69.094008, arXiv:hep-ph/0312266.
- [40] S. Dittmaier, A. Huss, and C. Schwinn, “Mixed QCD-electroweak $O(\alpha_s\alpha)$ corrections to Drell–Yan processes in the resonance region: pole approximation and non-factorizable corrections”, *Nucl. Phys. B* **885** (2014) 318, doi:10.1016/j.nuclphysb.2014.05.027, arXiv:1403.3216.
- [41] J. M. Lindert et al., “Precise predictions for V+jets dark matter backgrounds”, *Eur. Phys. J. C* **77** (2017) 829, doi:10.1140/epjc/s10052-017-5389-1, arXiv:1705.04664.
- [42] M. V. Garzelli, A. Kardos, C. G. Papadopoulos, and Z. Trocsanyi, “ $t\bar{t}W^\pm$ and $t\bar{t}Z$ hadroproduction at NLO accuracy in QCD with parton shower and hadronization effects”, *JHEP* **11** (2012) 056, doi:10.1007/JHEP11(2012)056, arXiv:1208.2665.

-
- [43] S. Frixione et al., “Electroweak and QCD corrections to top-pair hadroproduction in association with heavy bosons”, *JHEP* **06** (2015) 184, doi:10.1007/JHEP06(2015)184, arXiv:1504.03446.
- [44] T. Gehrmann et al., “ W^+W^- production at hadron colliders in next to next to leading order QCD”, *Phys. Rev. Lett.* **113** (2014) 212001, doi:10.1103/PhysRevLett.113.212001, arXiv:1408.5243.
- [45] P. Skands, S. Carrazza, and J. Rojo, “Tuning PYTHIA 8.1: the Monash 2013 tune”, *Eur. Phys. J. C* **74** (2014) 3024, doi:10.1140/epjc/s10052-014-3024-y, arXiv:1404.5630.
- [46] CMS Collaboration, “Event generator tunes obtained from underlying event and multiparton scattering measurements”, *Eur. Phys. J. C* **76** (2016) 155, doi:10.1140/epjc/s10052-016-3988-x, arXiv:1512.00815.
- [47] CMS Collaboration, “Extraction and validation of a new set of CMS PYTHIA8 tunes from underlying-event measurements”, *Eur. Phys. J. C* **80** (2020) 4, doi:10.1140/epjc/s10052-019-7499-4, arXiv:1903.12179.
- [48] NNPDF Collaboration, “Parton distributions from high-precision collider data”, *Eur. Phys. J. C* **77** (2017) 663, doi:10.1140/epjc/s10052-017-5199-5, arXiv:1706.00428.
- [49] NNPDF Collaboration, “Parton distributions for the LHC Run II”, *JHEP* **04** (2015) 040, doi:10.1007/JHEP04(2015)040, arXiv:1410.8849.
- [50] J. Alwall et al., “Comparative study of various algorithms for the merging of parton showers and matrix elements in hadronic collisions”, *Eur. Phys. J. C* **53** (2008) 473, doi:10.1140/epjc/s10052-007-0490-5, arXiv:0706.2569.
- [51] R. Frederix and S. Frixione, “Merging meets matching in MC@NLO”, *JHEP* **12** (2012) 061, doi:10.1007/JHEP12(2012)061, arXiv:1209.6215.
- [52] GEANT4 Collaboration, “GEANT4—a simulation toolkit”, *Nucl. Instrum. Meth. A* **506** (2003) 250, doi:10.1016/S0168-9002(03)01368-8.
- [53] CMS Collaboration, “Measurement of the inelastic proton-proton cross section at $\sqrt{s} = 13$ TeV”, *JHEP* **07** (2018) 161, doi:10.1007/JHEP07(2018)161, arXiv:1802.02613.
- [54] CMS Collaboration, “Particle-flow reconstruction and global event description with the CMS detector”, *JINST* **12** (2017) P10003, doi:10.1088/1748-0221/12/10/P10003, arXiv:1706.04965.
- [55] CMS Collaboration, “Performance of the CMS muon detector and muon reconstruction with proton-proton collisions at $\sqrt{s} = 13$ TeV”, *JINST* **13** (2018) P06015, doi:10.1088/1748-0221/13/06/P06015, arXiv:1804.04528.
- [56] CMS Collaboration, “Performance of electron reconstruction and selection with the CMS detector in proton-proton collisions at $\sqrt{s} = 8$ TeV”, *JINST* **10** (2015) P06005, doi:10.1088/1748-0221/10/06/P06005, arXiv:1502.02701.

- [57] CMS Collaboration, “Performance of photon reconstruction and identification with the CMS detector in proton-proton collisions at $\sqrt{s} = 8$ TeV”, *JINST* **10** (2015) P08010, doi:10.1088/1748-0221/10/08/P08010, arXiv:1502.02702.
- [58] CMS Collaboration, “Electron and photon reconstruction and identification with the CMS experiment at the CERN LHC”, *JINST* **16** (2021) P05014, doi:10.1088/1748-0221/16/05/P05014, arXiv:2012.06888.
- [59] CMS Collaboration, “Performance of CMS muon reconstruction in pp collision events at $\sqrt{s} = 7$ TeV”, *JINST* **7** (2012) P10002, doi:10.1088/1748-0221/7/10/P10002, arXiv:1206.4071.
- [60] M. Cacciari, G. P. Salam, and G. Soyez, “The anti- k_T jet clustering algorithm”, *JHEP* **04** (2008) 063, doi:10.1088/1126-6708/2008/04/063, arXiv:0802.1189.
- [61] M. Cacciari, G. P. Salam, and G. Soyez, “FastJet user manual”, *Eur. Phys. J. C* **72** (2012) 1896, doi:10.1140/epjc/s10052-012-1896-2, arXiv:1111.6097.
- [62] CMS Collaboration, “Jet energy scale and resolution in the CMS experiment in pp collisions at 8 TeV”, *JINST* **12** (2017) P02014, doi:10.1088/1748-0221/12/02/P02014, arXiv:1607.03663.
- [63] CMS Collaboration, “Identification of heavy-flavour jets with the CMS detector in pp collisions at 13 TeV”, *JINST* **13** (2018) P05011, doi:10.1088/1748-0221/13/05/P05011, arXiv:1712.07158.
- [64] CMS Collaboration, “Measurement of the differential Drell–Yan cross section in proton-proton collisions at $\sqrt{s} = 13$ TeV”, *JHEP* **12** (2019) 059, doi:10.1007/JHEP12(2019)059, arXiv:1812.10529.
- [65] M. Cacciari and G. P. Salam, “Pileup subtraction using jet areas”, *Phys. Lett. B* **659** (2008) 119, doi:10.1016/j.physletb.2007.09.077, arXiv:0707.1378.
- [66] CMS Collaboration, “Measurement of the top-antitop production cross section in pp collisions at $\sqrt{s} = 7$ TeV using the kinematic properties of events with leptons and jets”, *Eur. Phys. J. C* **71** (2011) 1721, doi:10.1140/epjc/s10052-011-1721-3, arXiv:1106.0902.
- [67] Particle Data Group, P. A. Zyla et al., “Review of particle physics”, *Prog. Theor. Exp. Phys.* **2020** (2020) 083C01, doi:10.1093/ptep/ptaa104.
- [68] The ATLAS Collaboration, The CMS Collaboration, The LHC Higgs Combination Group, “Procedure for the LHC Higgs boson search combination in Summer 2011”, Technical Report CMS-NOTE-2011-005, ATL-PHYS-PUB-2011-11, 2011.
- [69] G. Cowan, K. Cranmer, E. Gross, and O. Vitells, “Asymptotic formulae for likelihood-based tests of new physics”, *Eur. Phys. J. C* **71** (2011) 1554, doi:10.1140/epjc/s10052-011-1554-0, arXiv:1007.1727. [Erratum: doi:10.1140/epjc/s10052-013-2501-z].
- [70] CMS Collaboration, “Precision luminosity measurement in proton-proton collisions at $\sqrt{s} = 13$ TeV in 2015 and 2016 at CMS”, 2021. arXiv:2104.01927. Submitted to EPJC.
- [71] CMS Collaboration, “CMS luminosity measurement for the 2017 data-taking period at $\sqrt{s} = 13$ TeV”, Technical Report CMS-PAS-LUM-17-004, 2018.

- [72] CMS Collaboration, “CMS luminosity measurement for the 2018 data-taking period at $\sqrt{s} = 13$ TeV”, Technical Report CMS-PAS-LUM-18-002, 2019.
- [73] ATLAS Collaboration, “Measurement of the inelastic proton-proton cross section at $\sqrt{s} = 13$ TeV with the ATLAS detector at the LHC”, *Phys. Rev. Lett.* **117** (2016) 182002, doi:10.1103/PhysRevLett.117.182002, arXiv:1606.02625.
- [74] CMS Collaboration, “Energy calibration and resolution of the CMS electromagnetic calorimeter in pp collisions at $\sqrt{s} = 7$ TeV”, *JINST* **8** (2013) P09009, doi:10.1088/1748-0221/8/09/P09009, arXiv:1306.2016.
- [75] CMS Collaboration, “Identification of b-quark jets with the CMS experiment”, *JINST* **8** (2013) P04013, doi:10.1088/1748-0221/8/04/P04013, arXiv:1211.4462.
- [76] R. J. Barlow and C. Beeston, “Fitting using finite Monte Carlo samples”, *Comput. Phys. Commun.* **77** (1993) 219, doi:10.1016/0010-4655(93)90005-W.
- [77] S. Argyropoulos and T. Sjöstrand, “Effects of color reconnection on $t\bar{t}$ final states at the LHC”, *JHEP* **11** (2014) 043, doi:10.1007/JHEP11(2014)043, arXiv:1407.6653.
- [78] J. R. Christiansen and P. Z. Skands, “String formation beyond leading colour”, *JHEP* **08** (2015) 003, doi:10.1007/JHEP08(2015)003, arXiv:1505.01681.
- [79] G. Cowan, “Statistical data analysis”. Clarendon Press, 1998.
- [80] S. Schmitt, “TUnfold, an algorithm for correcting migration effects in high energy physics”, *JINST* **7** (2012) T10003, doi:10.1088/1748-0221/7/10/T10003, arXiv:1205.6201.
- [81] J. Bellm et al., “Herwig 7.0/Herwig++ 3.0 release note”, *Eur. Phys. J. C* **76** (2016) 196, doi:10.1140/epjc/s10052-016-4018-8, arXiv:1512.01178.
- [82] CMS Collaboration, “Development and validation of HERWIG 7 tunes from CMS underlying-event measurements”, *Eur. Phys. J. C* **81** (2021) 312, doi:10.1140/epjc/s10052-021-08949-5, arXiv:2011.03422.
- [83] W. Hollik et al., “Top dipole form-factors and loop induced CP violation in supersymmetry”, *Nucl. Phys. B* **551** (1999) 3, doi:10.1016/S0550-3213(99)00201-1, arXiv:hep-ph/9812298. [Erratum: doi:10.1016/S0550-3213(99)00396-X].
- [84] K. Agashe, G. Perez, and A. Soni, “Collider signals of top quark flavor violation from a warped extra dimension”, *Phys. Rev. D* **75** (2007) 015002, doi:10.1103/PhysRevD.75.015002, arXiv:hep-ph/0606293.
- [85] A. L. Kagan, G. Perez, T. Volansky, and J. Zupan, “General minimal flavor violation”, *Phys. Rev. D* **80** (2009) 076002, doi:10.1103/PhysRevD.80.076002, arXiv:0903.1794.
- [86] T. Ibrahim and P. Nath, “The top quark electric dipole moment in an MSSM extension with vector like multiplets”, *Phys. Rev. D* **82** (2010) 055001, doi:10.1103/PhysRevD.82.055001, arXiv:1007.0432.
- [87] T. Ibrahim and P. Nath, “The chromoelectric dipole moment of the top quark in models with vector like multiplets”, *Phys. Rev. D* **84** (2011) 015003, doi:10.1103/PhysRevD.84.015003, arXiv:1104.3851.

- [88] C. Grojean, O. Matsedonskyi, and G. Panico, “Light top partners and precision physics”, *JHEP* **10** (2013) 160, doi:10.1007/JHEP10(2013)160, arXiv:1306.4655.
- [89] F. Richard, “Can LHC observe an anomaly in $t\bar{t}Z$ production?”, 2013. arXiv:1304.3594.
- [90] B. Grzadkowski, M. Iskrzynski, M. Misiak, and J. Rosiek, “Dimension-six terms in the standard model Lagrangian”, *JHEP* **10** (2010) 085, doi:10.1007/JHEP10(2010)085, arXiv:1008.4884.
- [91] C. Zhang and S. Willenbrock, “Effective-field-theory approach to top-quark production and decay”, *Phys. Rev. D* **83** (2011) 034006, doi:10.1103/PhysRevD.83.034006, arXiv:1008.3869.
- [92] CMS Collaboration, “Measurements of $t\bar{t}$ differential cross sections in proton-proton collisions at $\sqrt{s} = 13$ TeV using events containing two leptons”, *JHEP* **02** (2019) 149, doi:10.1007/JHEP02(2019)149, arXiv:1811.06625.
- [93] CMS Collaboration, “Measurement of the top quark polarization and $t\bar{t}$ spin correlations using dilepton final states in proton-proton collisions at $\sqrt{s} = 13$ TeV”, *Phys. Rev. D* **100** (2019) 072002, doi:10.1103/PhysRevD.100.072002, arXiv:1907.03729.
- [94] CMS Collaboration, “Measurement of the W boson helicity fractions in the decays of top quark pairs to lepton+jets final states produced in pp collisions at $\sqrt{s} = 8$ TeV”, *Phys. Lett. B* **762** (2016) 512, doi:10.1016/j.physletb.2016.10.007, arXiv:1605.09047.
- [95] J. A. Aguilar-Saavedra and J. Bernabeu, “W polarisation beyond helicity fractions in top quark decays”, *Nucl. Phys. B* **840** (2010) 349, doi:10.1016/j.nuclphysb.2010.07.012, arXiv:1005.5382.
- [96] CMS Collaboration, “Search for new physics in top quark production with additional leptons in proton-proton collisions at $\sqrt{s} = 13$ TeV using effective field theory”, *JHEP* **03** (2021) 095, doi:10.1007/JHEP03(2021)095, arXiv:2012.04120.
- [97] CMS Collaboration, “Measurement of top quark pair production in association with a Z boson in proton-proton collisions at $\sqrt{s} = 13$ TeV”, *JHEP* **03** (2020) 056, doi:10.1007/JHEP03(2020)056, arXiv:1907.11270.
- [98] ATLAS Collaboration, “Measurement of the $t\bar{t}Z$ and $t\bar{t}W$ cross sections in proton-proton collisions at $\sqrt{s} = 13$ TeV with the ATLAS detector”, *Phys. Rev. D* **99** (2019) 072009, doi:10.1103/PhysRevD.99.072009, arXiv:1901.03584.
- [99] CMS Collaboration, “Measurement of the cross section for top quark pair production in association with a W or Z boson in proton-proton collisions at $\sqrt{s} = 13$ TeV”, *JHEP* **08** (2018) 011, doi:10.1007/JHEP08(2018)011, arXiv:1711.02547.
- [100] J. Ellis et al., “Top, Higgs, diboson and electroweak fit to the standard model effective field theory”, *JHEP* **04** (2021) 279, doi:10.1007/JHEP04(2021)279, arXiv:2012.02779.

A The CMS Collaboration

Yerevan Physics Institute, Yerevan, Armenia

A. Tumasyan

Institut für Hochenergiephysik, Wien, Austria

W. Adam, J.W. Andrejkovic, T. Bergauer, S. Chatterjee, M. Dragicevic, A. Escalante Del Valle, R. Frühwirth¹, M. Jeitler¹, N. Krammer, L. Lechner, D. Liko, I. Mikulec, P. Paulitsch, F.M. Pitters, J. Schieck¹, R. Schöfbeck, M. Spanring, S. Templ, W. Waltenberger, C.-E. Wulz¹

Institute for Nuclear Problems, Minsk, Belarus

V. Chekhovsky, A. Litomin, V. Makarenko

Universiteit Antwerpen, Antwerpen, Belgium

M.R. Darwish², E.A. De Wolf, X. Janssen, T. Kello³, A. Lelek, H. Rejeb Sfar, P. Van Mechelen, S. Van Putte, N. Van Remortel

Vrije Universiteit Brussel, Brussel, Belgium

F. Blekman, E.S. Bols, J. D'Hondt, J. De Clercq, M. Delcourt, H. El Faham, S. Lowette, S. Moortgat, A. Morton, D. Müller, A.R. Sahasransu, S. Tavernier, W. Van Doninck, P. Van Mulders

Université Libre de Bruxelles, Bruxelles, Belgium

D. Beghin, B. Bilin, B. Clerboux, G. De Lentdecker, L. Favart, A. Grebenyuk, A.K. Kalsi, K. Lee, M. Mahdavihorrami, I. Makarenko, L. Moureaux, L. Pétré, A. Popov, N. Postiau, E. Starling, L. Thomas, M. Vanden Bemden, C. Vander Velde, P. Vanlaer, D. Vannerom, L. Wezenbeek

Ghent University, Ghent, Belgium

T. Cornelis, D. Dobur, J. Knolle, L. Lambrecht, G. Mestdach, M. Niedziela, C. Roskas, A. Samalan, K. Skovpen, M. Tytgat, W. Verbeke, B. Vermassen, M. Vit

Université Catholique de Louvain, Louvain-la-Neuve, Belgium

A. Bethani, G. Bruno, F. Bury, C. Caputo, P. David, C. Delaere, I.S. Donertas, A. Giammanco, K. Jaffel, Sa. Jain, V. Lemaître, K. Mondal, J. Prisciandaro, A. Taliercio, M. Teklishyn, T.T. Tran, P. Vischia, S. Wertz

Centro Brasileiro de Pesquisas Físicas, Rio de Janeiro, Brazil

G.A. Alves, C. Hensel, A. Moraes

Universidade do Estado do Rio de Janeiro, Rio de Janeiro, Brazil

W.L. Aldá Júnior, M. Alves Gallo Pereira, M. Barroso Ferreira Filho, H. BRANDAO MALBOUISSON, W. Carvalho, J. Chinellato⁴, E.M. Da Costa, G.G. Da Silveira⁵, D. De Jesus Damiao, S. Fonseca De Souza, D. Matos Figueiredo, C. Mora Herrera, K. Mota Amarilo, L. Mundim, H. Nogima, P. Rebello Teles, A. Santoro, S.M. Silva Do Amaral, A. Sznajder, M. Thiel, F. Torres Da Silva De Araujo, A. Vilela Pereira

Universidade Estadual Paulista ^a, Universidade Federal do ABC ^b, São Paulo, Brazil

C.A. Bernardes^{a,a,5}, L. Calligaris^a, T.R. Fernandez Perez Tomei^a, E.M. Gregores^{a,b}, D.S. Lemos^a, P.G. Mercadante^{a,b}, S.F. Novaes^a, Sandra S. Padula^a

Institute for Nuclear Research and Nuclear Energy, Bulgarian Academy of Sciences, Sofia, Bulgaria

A. Aleksandrov, G. Antchev, R. Hadjiiska, P. Iaydjiev, M. Misheva, M. Rodozov, M. Shopova, G. Sultanov

University of Sofia, Sofia, Bulgaria

A. Dimitrov, T. Ivanov, L. Litov, B. Pavlov, P. Petkov, A. Petrov

Beihang University, Beijing, China

T. Cheng, Q. Guo, T. Javaid⁶, M. Mittal, H. Wang, L. Yuan

Department of Physics, Tsinghua University, Beijing, China

M. Ahmad, G. Bauer, C. Dozen⁷, Z. Hu, J. Martins⁸, Y. Wang, K. Yi^{9,10}

Institute of High Energy Physics, Beijing, China

E. Chapon, G.M. Chen⁶, H.S. Chen⁶, M. Chen, F. Iemmi, A. Kapoor, D. Leggat, H. Liao, Z.-A. LIU⁶, V. Milosevic, F. Monti, R. Sharma, J. Tao, J. Thomas-wilsker, J. Wang, H. Zhang, S. Zhang⁶, J. Zhao

State Key Laboratory of Nuclear Physics and Technology, Peking University, Beijing, China

A. Agapitos, Y. Ban, C. Chen, Q. Huang, A. Levin, Q. Li, X. Lyu, Y. Mao, S.J. Qian, D. Wang, Q. Wang, J. Xiao

Sun Yat-Sen University, Guangzhou, China

M. Lu, Z. You

Institute of Modern Physics and Key Laboratory of Nuclear Physics and Ion-beam Application (MOE) - Fudan University, Shanghai, China

X. Gao³, H. Okawa

Zhejiang University, Hangzhou, China

Z. Lin, M. Xiao

Universidad de Los Andes, Bogota, Colombia

C. Avila, A. Cabrera, C. Florez, J. Fraga, A. Sarkar, M.A. Segura Delgado

Universidad de Antioquia, Medellin, Colombia

J. Mejia Guisao, F. Ramirez, J.D. Ruiz Alvarez, C.A. Salazar González

University of Split, Faculty of Electrical Engineering, Mechanical Engineering and Naval Architecture, Split, Croatia

D. Giljanovic, N. Godinovic, D. Lelas, I. Puljak

University of Split, Faculty of Science, Split, Croatia

Z. Antunovic, M. Kovac, T. Sculac

Institute Rudjer Boskovic, Zagreb, Croatia

V. Brigljevic, D. Ferencek, D. Majumder, M. Roguljic, A. Starodumov¹¹, T. Susa

University of Cyprus, Nicosia, Cyprus

A. Attikis, K. Christoforou, E. Erodotou, A. Ioannou, G. Kole, M. Kolosova, S. Konstantinou, J. Mousa, C. Nicolaou, F. Ptochos, P.A. Razis, H. Rykaczewski, H. Saka

Charles University, Prague, Czech Republic

M. Finger¹², M. Finger Jr.¹², A. Kveton

Escuela Politecnica Nacional, Quito, Ecuador

E. Ayala

Universidad San Francisco de Quito, Quito, Ecuador

E. Carrera Jarrin

Academy of Scientific Research and Technology of the Arab Republic of Egypt, Egyptian Network of High Energy Physics, Cairo, Egypt

H. Abdalla¹³, S. Khalil¹⁴

Center for High Energy Physics (CHEP-FU), Fayoum University, El-Fayoum, Egypt

A. Lotfy, M.A. Mahmoud

National Institute of Chemical Physics and Biophysics, Tallinn, Estonia

S. Bhowmik, A. Carvalho Antunes De Oliveira, R.K. Dewanjee, K. Ehataht, M. Kadastik, S. Nandan, C. Nielsen, J. Pata, M. Raidal, L. Tani, C. Veelken

Department of Physics, University of Helsinki, Helsinki, Finland

P. Eerola, L. Forthomme, H. Kirschenmann, K. Osterberg, M. Voutilainen

Helsinki Institute of Physics, Helsinki, Finland

S. Bharthuar, E. Brücken, F. Garcia, J. Havukainen, M.S. Kim, R. Kinnunen, T. Lampén, K. Lassila-Perini, S. Lehti, T. Lindén, M. Lotti, L. Martikainen, M. Myllymäki, J. Ott, H. Siikonen, E. Tuominen, J. Tuominiemi

Lappeenranta University of Technology, Lappeenranta, Finland

P. Luukka, H. Petrow, T. Tuuva

IRFU, CEA, Université Paris-Saclay, Gif-sur-Yvette, France

C. Amendola, M. Besancon, F. Couderc, M. Dejardin, D. Denegri, J.L. Faure, F. Ferri, S. Ganjour, A. Givernaud, P. Gras, G. Hamel de Monchenault, P. Jarry, B. Lenzi, E. Locci, J. Malcles, J. Rander, A. Rosowsky, M.Ö. Sahin, A. Savoy-Navarro¹⁵, M. Titov, G.B. Yu

Laboratoire Leprince-Ringuet, CNRS/IN2P3, Ecole Polytechnique, Institut Polytechnique de Paris, Palaiseau, France

S. Ahuja, F. Beaudette, M. Bonanomi, A. Buchot Perraguin, P. Busson, A. Cappati, C. Charlot, O. Davignon, B. Diab, G. Falmagne, S. Ghosh, R. Granier de Cassagnac, A. Hakimi, I. Kucher, M. Nguyen, C. Ochando, P. Paganini, J. Rembser, R. Salerno, J.B. Sauvan, Y. Sirois, A. Zabi, A. Zghiche

Université de Strasbourg, CNRS, IPHC UMR 7178, Strasbourg, France

J.-L. Agram¹⁶, J. Andrea, D. Apparau, D. Bloch, G. Bourgatte, J.-M. Brom, E.C. Chabert, C. Collard, D. Darej, J.-C. Fontaine¹⁶, U. Goerlach, C. Grimault, A.-C. Le Bihan, E. Nibigira, P. Van Hove

Institut de Physique des 2 Infinis de Lyon (IP2I), Villeurbanne, France

E. Asilar, S. Beauceron, C. Bernet, G. Boudoul, C. Camen, A. Carle, N. Chanon, D. Contardo, P. Depasse, H. El Mamouni, J. Fay, S. Gascon, M. Gouzevitch, B. Ille, I.B. Laktineh, H. Lattaud, A. Lesauvage, M. Lethuillier, L. Mirabito, S. Perries, K. Shchablo, V. Sordini, L. Torterotot, G. Touquet, M. Vander Donckt, S. Viret

Georgian Technical University, Tbilisi, Georgia

I. Lomidze, T. Toriashvili¹⁷, Z. Tsamalaidze¹²

RWTH Aachen University, I. Physikalisches Institut, Aachen, Germany

L. Feld, K. Klein, M. Lipinski, D. Meuser, A. Pauls, M.P. Rauch, N. Röwert, J. Schulz, M. Teroerde

RWTH Aachen University, III. Physikalisches Institut A, Aachen, Germany

A. Dodonova, D. Eliseev, M. Erdmann, P. Fackeldey, B. Fischer, S. Ghosh, T. Hebbeker, K. Hoepfner, F. Ivone, H. Keller, L. Mastrolorenzo, M. Merschmeyer, A. Meyer, G. Mocellin,

S. Mondal, S. Mukherjee, D. Noll, A. Novak, T. Pook, A. Pozdnyakov, Y. Rath, H. Reithler, J. Roemer, A. Schmidt, S.C. Schuler, A. Sharma, L. Vigilante, S. Wiedenbeck, S. Zaleski

RWTH Aachen University, III. Physikalisches Institut B, Aachen, Germany

C. Dziwok, G. Flügge, W. Haj Ahmad¹⁸, O. Hlushchenko, T. Kress, A. Nowack, C. Pistone, O. Pooth, D. Roy, H. Sert, A. Stahl¹⁹, T. Ziemons

Deutsches Elektronen-Synchrotron, Hamburg, Germany

H. Aarup Petersen, M. Aldaya Martin, P. Asmuss, I. Babounikau, S. Baxter, O. Behnke, A. Bermúdez Martínez, S. Bhattacharya, A.A. Bin Anuar, K. Borras²⁰, V. Botta, D. Brunner, A. Campbell, A. Cardini, C. Cheng, F. Colombina, S. Consuegra Rodríguez, G. Correia Silva, V. Danilov, L. Didukh, G. Eckerlin, D. Eckstein, L.I. Estevez Banos, O. Filatov, E. Gallo²¹, A. Geiser, A. Giraldi, A. Grohsjean, M. Guthoff, A. Jafari²², N.Z. Jomhari, H. Jung, A. Kasem²⁰, M. Kasemann, H. Kaveh, C. Kleinwort, D. Krücker, W. Lange, J. Lidrych, K. Lipka, W. Lohmann²³, R. Mankel, I.-A. Melzer-Pellmann, J. Metwally, A.B. Meyer, M. Meyer, J. Mnich, A. Mussgiller, Y. Otariid, D. Pérez Adán, D. Pitzl, A. Raspereza, B. Ribeiro Lopes, J. Rübenach, A. Saggio, A. Saibel, M. Savitskyi, M. Scham, V. Scheurer, C. Schwanenberger²¹, A. Singh, R.E. Sosa Ricardo, D. Stafford, N. Tonon, O. Turkot, M. Van De Klundert, R. Walsh, D. Walter, Y. Wen, K. Wichmann, L. Wiens, C. Wissing, S. Wuchterl

University of Hamburg, Hamburg, Germany

R. Aggleton, S. Albrecht, S. Bein, L. Benato, A. Benecke, P. Connor, K. De Leo, M. Eich, F. Feindt, A. Fröhlich, C. Garbers, E. Garutti, P. Gunnellini, J. Haller, A. Hinzmann, G. Kasieczka, R. Klanner, R. Kogler, T. Kramer, V. Kutzner, J. Lange, T. Lange, A. Lobanov, A. Malara, A. Nigamova, K.J. Pena Rodriguez, O. Rieger, P. Schleper, M. Schröder, J. Schwandt, D. Schwarz, J. Sonneveld, H. Stadie, G. Steinbrück, A. Tews, B. Vormwald, I. Zoi

Karlsruher Institut fuer Technologie, Karlsruhe, Germany

J. Bechtel, T. Berger, E. Butz, R. Caspart, T. Chwalek, W. De Boer[†], A. Dierlamm, A. Droll, K. El Morabit, N. Faltermann, M. Giffels, J.o. Gosewisch, A. Gottmann, F. Hartmann¹⁹, C. Heidecker, U. Husemann, I. Katkov²⁴, P. Keicher, R. Koppenhöfer, S. Maier, M. Metzler, S. Mitra, Th. Müller, M. Neukum, A. Nürnberg, G. Quast, K. Rabbertz, J. Rauser, D. Savoii, M. Schnepf, D. Seith, I. Shvetsov, H.J. Simonis, R. Ulrich, J. Van Der Linden, R.F. Von Cube, M. Wassmer, M. Weber, S. Wieland, R. Wolf, S. Wozniewski, S. Wunsch

Institute of Nuclear and Particle Physics (INPP), NCSR Demokritos, Aghia Paraskevi, Greece

G. Anagnostou, G. Daskalakis, T. Geralis, A. Kyriakis, D. Loukas, A. Stakia

National and Kapodistrian University of Athens, Athens, Greece

M. Diamantopoulou, D. Karasavvas, G. Karathanasis, P. Kontaxakis, C.K. Koraka, A. Manousakis-katsikakis, A. Panagiotou, I. Papavergou, N. Saoulidou, K. Theofilatos, E. Tziaferi, K. Vellidis, E. Vourliotis

National Technical University of Athens, Athens, Greece

G. Bakas, K. Kousouris, I. Papakrivopoulos, G. Tsipolitis, A. Zacharopoulou

University of Ioánnina, Ioánnina, Greece

I. Evangelou, C. Foudas, P. Gianneios, P. Katsoulis, P. Kokkas, N. Manthos, I. Papadopoulos, J. Strologas

MTA-ELTE Lendület CMS Particle and Nuclear Physics Group, Eötvös Loránd University,

Budapest, Hungary

M. Csanad, K. Farkas, M.M.A. Gadallah²⁵, S. Lökös²⁶, P. Major, K. Mandal, A. Mehta, G. Pasztor, A.J. Rádl, O. Surányi, G.I. Veres

Wigner Research Centre for Physics, Budapest, Hungary

M. Bartók²⁷, G. Bencze, C. Hajdu, D. Horvath²⁸, F. Sikler, V. Veszpremi, G. Vesztergombi[†]

Institute of Nuclear Research ATOMKI, Debrecen, Hungary

S. Czellar, J. Karancsi²⁷, J. Molnar, Z. Szillasi, D. Teyssier

Institute of Physics, University of Debrecen, Debrecen, Hungary

P. Raics, Z.L. Trocsanyi²⁹, B. Ujvari

Karoly Robert Campus, MATE Institute of Technology

T. Csorgo³⁰, F. Nemes³⁰, T. Novak

Indian Institute of Science (IISc), Bangalore, India

J.R. Komaragiri, D. Kumar, L. Panwar, P.C. Tiwari

National Institute of Science Education and Research, HBNI, Bhubaneswar, India

S. Bahinipati³¹, A.K. Das, C. Kar, P. Mal, T. Mishra, V.K. Muraleedharan Nair Bindhu³², A. Nayak³², P. Saha, N. Sur, S.K. Swain, D. Vats³²

Panjab University, Chandigarh, India

S. Bansal, S.B. Beri, V. Bhatnagar, G. Chaudhary, S. Chauhan, N. Dhingra³³, R. Gupta, A. Kaur, M. Kaur, S. Kaur, P. Kumari, M. Meena, K. Sandeep, J.B. Singh, A.K. Viridi

University of Delhi, Delhi, India

A. Ahmed, A. Bhardwaj, B.C. Choudhary, M. Gola, S. Keshri, A. Kumar, M. Naimuddin, P. Priyanka, K. Ranjan, A. Shah

Saha Institute of Nuclear Physics, HBNI, Kolkata, India

M. Bharti³⁴, R. Bhattacharya, S. Bhattacharya, D. Bhowmik, S. Dutta, S. Dutta, B. Gomber³⁵, M. Maity³⁶, P. Palit, P.K. Rout, G. Saha, B. Sahu, S. Sarkar, M. Sharan, B. Singh³⁴, S. Thakur³⁴

Indian Institute of Technology Madras, Madras, India

P.K. Behera, S.C. Behera, P. Kalbhor, A. Muhammad, R. Pradhan, P.R. Pujahari, A. Sharma, A.K. Sikdar

Bhabha Atomic Research Centre, Mumbai, India

D. Dutta, V. Jha, V. Kumar, D.K. Mishra, K. Naskar³⁷, P.K. Netrakanti, L.M. Pant, P. Shukla

Tata Institute of Fundamental Research-A, Mumbai, India

T. Aziz, S. Dugad, M. Kumar, U. Sarkar

Tata Institute of Fundamental Research-B, Mumbai, India

S. Banerjee, R. Chudasama, M. Guchait, S. Karmakar, S. Kumar, G. Majumder, K. Mazumdar, S. Mukherjee

Indian Institute of Science Education and Research (IISER), Pune, India

K. Alpana, S. Dube, B. Kansal, A. Laha, S. Pandey, A. Rane, A. Rastogi, S. Sharma

Department of Physics, Isfahan University of Technology, Isfahan, Iran

H. Bakhshiansohi³⁸, M. Zeinali³⁹

Institute for Research in Fundamental Sciences (IPM), Tehran, Iran

S. Chenarani⁴⁰, S.M. Etesami, M. Khakzad, M. Mohammadi Najafabadi

University College Dublin, Dublin, Ireland

M. Grunewald

INFN Sezione di Bari ^a, Università di Bari ^b, Politecnico di Bari ^c, Bari, Italy

M. Abbrescia^{a,b}, R. Aly^{a,b,41}, C. Aruta^{a,b}, A. Colaleo^a, D. Creanza^{a,c}, N. De Filippis^{a,c}, M. De Palma^{a,b}, A. Di Florio^{a,b}, A. Di Pilato^{a,b}, W. Elmetenawee^{a,b}, L. Fiore^a, A. Gelmi^{a,b}, M. Gul^a, G. Iaselli^{a,c}, M. Ince^{a,b}, S. Lezki^{a,b}, G. Maggi^{a,c}, M. Maggi^a, I. Margjeka^{a,b}, V. Mastrapasqua^{a,b}, J.A. Merlin^a, S. My^{a,b}, S. Nuzzo^{a,b}, A. Pellecchia^{a,b}, A. Pompili^{a,b}, G. Pugliese^{a,c}, A. Ranieri^a, G. Selvaggi^{a,b}, L. Silvestris^a, F.M. Simone^{a,b}, R. Venditti^a, P. Verwilligen^a

INFN Sezione di Bologna ^a, Università di Bologna ^b, Bologna, Italy

G. Abbiendi^a, C. Battilana^{a,b}, D. Bonacorsi^{a,b}, L. Borgonovi^a, L. Brigliadori^a, R. Campanini^{a,b}, P. Capiluppi^{a,b}, A. Castro^{a,b}, F.R. Cavallo^a, M. Cuffiani^{a,b}, G.M. Dallavalle^a, T. Diotallevi^{a,b}, F. Fabbrì^a, A. Fanfani^{a,b}, P. Giacomelli^a, L. Giommi^{a,b}, C. Grandi^a, L. Guiducci^{a,b}, S. Lo Meo^{a,42}, L. Lunerti^{a,b}, S. Marcellini^a, G. Masetti^a, F.L. Navarria^{a,b}, A. Perrotta^a, F. Primavera^{a,b}, A.M. Rossi^{a,b}, T. Rovelli^{a,b}, G.P. Siroli^{a,b}

INFN Sezione di Catania ^a, Università di Catania ^b, Catania, Italy

S. Albergo^{a,b,43}, S. Costa^{a,b,43}, A. Di Mattia^a, R. Potenza^{a,b}, A. Tricomi^{a,b,43}, C. Tuve^{a,b}

INFN Sezione di Firenze ^a, Università di Firenze ^b, Firenze, Italy

G. Barbagli^a, A. Cassese^a, R. Ceccarelli^{a,b}, V. Ciulli^{a,b}, C. Civinini^a, R. D'Alessandro^{a,b}, E. Focardi^{a,b}, G. Latino^{a,b}, P. Lenzi^{a,b}, M. Lizzo^{a,b}, M. Meschini^a, S. Paoletti^a, R. Seidita^{a,b}, G. Sguazzoni^a, L. Viliani^a

INFN Laboratori Nazionali di Frascati, Frascati, Italy

L. Benussi, S. Bianco, D. Piccolo

INFN Sezione di Genova ^a, Università di Genova ^b, Genova, Italy

M. Bozzo^{a,b}, F. Ferro^a, R. Mulargia^{a,b}, E. Robutti^a, S. Tosi^{a,b}

INFN Sezione di Milano-Bicocca ^a, Università di Milano-Bicocca ^b, Milano, Italy

A. Benaglia^a, F. Brivio^{a,b}, F. Cetorelli^{a,b}, V. Ciriolo^{a,b,19}, F. De Guio^{a,b}, M.E. Dinardo^{a,b}, P. Dini^a, S. Gennai^a, A. Ghezzi^{a,b}, P. Govoni^{a,b}, L. Guzzi^{a,b}, M. Malberti^a, S. Malvezzi^a, A. Massironi^a, D. Menasce^a, L. Moroni^a, M. Paganoni^{a,b}, D. Pedrini^a, S. Ragazzi^{a,b}, N. Redaelli^a, T. Tabarelli de Fatis^{a,b}, D. Valsecchi^{a,b,19}, D. Zuolo^{a,b}

INFN Sezione di Napoli ^a, Università di Napoli 'Federico II' ^b, Napoli, Italy, Università della Basilicata ^c, Potenza, Italy, Università G. Marconi ^d, Roma, Italy

S. Buontempo^a, F. Carnevali^{a,b}, N. Cavallo^{a,c}, A. De Iorio^{a,b}, F. Fabozzi^{a,c}, A.O.M. Iorio^{a,b}, L. Lista^{a,b}, S. Meola^{a,d,19}, P. Paolucci^{a,19}, B. Rossi^a, C. Sciacca^{a,b}

INFN Sezione di Padova ^a, Università di Padova ^b, Padova, Italy, Università di Trento ^c, Trento, Italy

P. Azzi^a, N. Bacchetta^a, D. Bisello^{a,b}, P. Bortignon^a, A. Bragagnolo^{a,b}, R. Carlin^{a,b}, P. Checchia^a, T. Dorigo^a, U. Dosselli^a, F. Gasparini^{a,b}, U. Gasparini^{a,b}, S.Y. Hoh^{a,b}, L. Layer^{a,44}, M. Margoni^{a,b}, A.T. Meneguzzo^{a,b}, J. Pazzini^{a,b}, M. Presilla^{a,b}, P. Ronchese^{a,b}, R. Rossin^{a,b}, F. Simonetto^{a,b}, G. Strong^a, M. Tosi^{a,b}, H. YARAR^{a,b}, M. Zanetti^{a,b}, P. Zotto^{a,b}, A. Zucchetta^{a,b}, G. Zumerle^{a,b}

INFN Sezione di Pavia ^a, Università di Pavia ^b, Pavia, Italy

C. Aime^{a,b}, A. Braghieri^a, S. Calzaferri^{a,b}, D. Fiorina^{a,b}, P. Montagna^{a,b}, S.P. Ratti^{a,b}, V. Re^a, C. Riccardi^{a,b}, P. Salvini^a, I. Vai^a, P. Vitulo^{a,b}

INFN Sezione di Perugia ^a, Università di Perugia ^b, Perugia, Italy

P. Asenov^{a,45}, G.M. Bilei^a, D. Ciangottini^{a,b}, L. Fanò^{a,b}, P. Lariccia^{a,b}, M. Magherini^b, G. Mantovani^{a,b}, V. Mariani^{a,b}, M. Menichelli^a, F. Moscatelli^{a,45}, A. Piccinelli^{a,b}, A. Rossi^{a,b}, A. Santocchia^{a,b}, D. Spiga^a, T. Tedeschi^{a,b}

INFN Sezione di Pisa ^a, Università di Pisa ^b, Scuola Normale Superiore di Pisa ^c, Pisa Italy, Università di Siena ^d, Siena, Italy

P. Azzurri^a, G. Bagliesi^a, V. Bertacchi^{a,c}, L. Bianchini^a, T. Boccali^a, E. Bossini^{a,b}, R. Castaldi^a, M.A. Ciocci^{a,b}, V. D'Amante^{a,d}, R. Dell'Orso^a, M.R. Di Domenico^{a,d}, S. Donato^a, A. Giassi^a, F. Ligabue^{a,c}, E. Manca^{a,c}, G. Mandorli^{a,c}, A. Messineo^{a,b}, F. Palla^a, S. Parolia^{a,b}, G. Ramirez-Sanchez^{a,c}, A. Rizzi^{a,b}, G. Rolandi^{a,c}, S. Roy Chowdhury^{a,c}, A. Scribano^a, N. Shafiei^{a,b}, P. Spagnolo^a, R. Tenchini^a, G. Tonelli^{a,b}, N. Turini^{a,d}, A. Venturi^a, P.G. Verdini^a

INFN Sezione di Roma ^a, Sapienza Università di Roma ^b, Rome, Italy

M. Campana^{a,b}, F. Cavallari^a, M. Cipriani^{a,b}, D. Del Re^{a,b}, E. Di Marco^a, M. Diemoz^a, E. Longo^{a,b}, P. Meridiani^a, G. Organtini^{a,b}, F. Pandolfi^a, R. Paramatti^{a,b}, C. Quaranta^{a,b}, S. Rahatlou^{a,b}, C. Rovelli^a, F. Santanastasio^{a,b}, L. Soffi^a, R. Tramontano^{a,b}

INFN Sezione di Torino ^a, Università di Torino ^b, Torino, Italy, Università del Piemonte Orientale ^c, Novara, Italy

N. Amapane^{a,b}, R. Arcidiacono^{a,c}, S. Argiro^{a,b}, M. Arneodo^{a,c}, N. Bartosik^a, R. Bellan^{a,b}, A. Bellora^{a,b}, J. Berenguer Antequera^{a,b}, C. Biino^a, N. Cartiglia^a, S. Cometti^a, M. Costa^{a,b}, R. Covarelli^{a,b}, N. Demaria^a, B. Kiani^{a,b}, F. Legger^a, C. Mariotti^a, S. Maselli^a, E. Migliore^{a,b}, E. Monteil^{a,b}, M. Monteno^a, M.M. Obertino^{a,b}, G. Ortona^a, L. Pacher^{a,b}, N. Pastrone^a, M. Pelliccioni^a, G.L. Pinna Angioni^{a,b}, M. Ruspa^{a,c}, K. Shchelina^{a,b}, F. Siviero^{a,b}, V. Sola^a, A. Solano^{a,b}, D. Soldi^{a,b}, A. Staiano^a, M. Tornago^{a,b}, D. Trocino^{a,b}, A. Vagnerini

INFN Sezione di Trieste ^a, Università di Trieste ^b, Trieste, Italy

S. Belforte^a, V. Candelise^{a,b}, M. Casarsa^a, F. Cossutti^a, A. Da Rold^{a,b}, G. Della Ricca^{a,b}, G. Sorrentino^{a,b}, F. Vazzoler^{a,b}

Kyungpook National University, Daegu, Korea

S. Dogra, C. Huh, B. Kim, D.H. Kim, G.N. Kim, J. Kim, J. Lee, S.W. Lee, C.S. Moon, Y.D. Oh, S.I. Pak, B.C. Radburn-Smith, S. Sekmen, Y.C. Yang

Chonnam National University, Institute for Universe and Elementary Particles, Kwangju, Korea

H. Kim, D.H. Moon

Hanyang University, Seoul, Korea

B. Francois, T.J. Kim, J. Park

Korea University, Seoul, Korea

S. Cho, S. Choi, Y. Go, B. Hong, K. Lee, K.S. Lee, J. Lim, J. Park, S.K. Park, J. Yoo

Kyung Hee University, Department of Physics, Seoul, Republic of Korea

J. Goh, A. Gurtu

Sejong University, Seoul, Korea

H.S. Kim, Y. Kim

Seoul National University, Seoul, Korea

J. Almond, J.H. Bhyun, J. Choi, S. Jeon, J. Kim, J.S. Kim, S. Ko, H. Kwon, H. Lee, S. Lee, B.H. Oh, M. Oh, S.B. Oh, H. Seo, U.K. Yang, I. Yoon

University of Seoul, Seoul, Korea

W. Jang, D. Jeon, D.Y. Kang, Y. Kang, J.H. Kim, S. Kim, B. Ko, J.S.H. Lee, Y. Lee, I.C. Park, Y. Roh, M.S. Ryu, D. Song, I.J. Watson, S. Yang

Yonsei University, Department of Physics, Seoul, Korea

S. Ha, H.D. Yoo

Sungkyunkwan University, Suwon, Korea

M. Choi, Y. Jeong, H. Lee, Y. Lee, I. Yu

College of Engineering and Technology, American University of the Middle East (AUM), Egaila, Kuwait

T. Beyrouthy, Y. Maghrbi

Riga Technical University, Riga, Latvia

T. Torims, V. Veckalns⁴⁶

Vilnius University, Vilnius, Lithuania

M. Ambrozias, A. Juodagalvis, A. Rinkevicius, G. Tamulaitis

National Centre for Particle Physics, Universiti Malaya, Kuala Lumpur, Malaysia

N. Bin Norjoharuddeen, W.A.T. Wan Abdullah, M.N. Yusli, Z. Zolkapli

Universidad de Sonora (UNISON), Hermosillo, Mexico

J.F. Benitez, A. Castaneda Hernandez, M. León Coello, J.A. Murillo Quijada, A. Sehwawat, L. Valencia Palomo

Centro de Investigacion y de Estudios Avanzados del IPN, Mexico City, Mexico

G. Ayala, H. Castilla-Valdez, E. De La Cruz-Burelo, I. Heredia-De La Cruz⁴⁷, R. Lopez-Fernandez, C.A. Mondragon Herrera, D.A. Perez Navarro, A. Sanchez-Hernandez

Universidad Iberoamericana, Mexico City, Mexico

S. Carrillo Moreno, C. Oropeza Barrera, M. Ramirez-Garcia, F. Vazquez Valencia

Benemerita Universidad Autonoma de Puebla, Puebla, Mexico

I. Pedraza, H.A. Salazar Ibarguen, C. Uribe Estrada

University of Montenegro, Podgorica, Montenegro

J. Mijuskovic⁴⁸, N. Raicevic

University of Auckland, Auckland, New Zealand

D. Krofcheck

University of Canterbury, Christchurch, New Zealand

S. Bheesette, P.H. Butler

National Centre for Physics, Quaid-I-Azam University, Islamabad, Pakistan

A. Ahmad, M.I. Asghar, A. Awais, M.I.M. Awan, H.R. Hoorani, W.A. Khan, M.A. Shah, M. Shoaib, M. Waqas

AGH University of Science and Technology Faculty of Computer Science, Electronics and Telecommunications, Krakow, Poland

V. Avati, L. Grzanka, M. Malawski

National Centre for Nuclear Research, Swierk, Poland

H. Bialkowska, M. Bluj, B. Boimska, M. Górski, M. Kazana, M. Szleper, P. Zalewski

Institute of Experimental Physics, Faculty of Physics, University of Warsaw, Warsaw, Poland
K. Bunkowski, K. Doroba, A. Kalinowski, M. Konecki, J. Krolikowski, M. Walczak

Laboratório de Instrumentação e Física Experimental de Partículas, Lisboa, Portugal
M. Araujo, P. Bargassa, D. Bastos, A. Boletti, P. Faccioli, M. Gallinaro, J. Hollar, N. Leonardo, T. Niknejad, M. Pisano, J. Seixas, O. Toldaiev, J. Varela

Joint Institute for Nuclear Research, Dubna, Russia
S. Afanasiev, D. Budkouski, I. Golutvin, I. Gorbunov, V. Karjavine, V. Korenkov, A. Lanev, A. Malakhov, V. Matveev^{49,50}, V. Palichik, V. Perelygin, M. Savina, D. Seitova, V. Shalaev, S. Shmatov, S. Shulha, V. Smirnov, O. Teryaev, N. Voytishin, B.S. Yuldashev⁵¹, A. Zarubin, I. Zhizhin

Petersburg Nuclear Physics Institute, Gatchina (St. Petersburg), Russia
G. Gavrillov, V. Golovtsov, Y. Ivanov, V. Kim⁵², E. Kuznetsova⁵³, V. Murzin, V. Oreshkin, I. Smirnov, D. Sosnov, V. Sulimov, L. Uvarov, S. Volkov, A. Vorobyev

Institute for Nuclear Research, Moscow, Russia
Yu. Andreev, A. Dermenev, S. Gninenko, N. Golubev, A. Karneyeu, D. Kirpichnikov, M. Kirsanov, N. Krasnikov, A. Pashenkov, G. Pivovarov, D. Tlisov[†], A. Toropin

Institute for Theoretical and Experimental Physics named by A.I. Alikhanov of NRC 'Kurchatov Institute', Moscow, Russia
V. Epshteyn, V. Gavrillov, N. Lychkovskaya, A. Nikitenko⁵⁴, V. Popov, A. Spiridonov, A. Stepenov, M. Toms, E. Vlasov, A. Zhokin

Moscow Institute of Physics and Technology, Moscow, Russia
T. Aushev

National Research Nuclear University 'Moscow Engineering Physics Institute' (MEPhI), Moscow, Russia
O. Bychkova, R. Chistov⁵⁵, M. Danilov⁵⁶, P. Parygin, S. Polikarpov⁵⁵

P.N. Lebedev Physical Institute, Moscow, Russia
V. Andreev, M. Azarkin, I. Dremin, M. Kirakosyan, A. Terkulov

Skobeltsyn Institute of Nuclear Physics, Lomonosov Moscow State University, Moscow, Russia
A. Belyaev, E. Boos, V. Bunichev, M. Dubinin⁵⁷, L. Dudko, A. Gribushin, V. Klyukhin, N. Korneeva, I. Lokhtin, S. Obraztsov, M. Perfilov, V. Savrin, P. Volkov

Novosibirsk State University (NSU), Novosibirsk, Russia
V. Blinov⁵⁸, T. Dimova⁵⁸, L. Kardapoltsev⁵⁸, A. Kozyrev⁵⁸, I. Ovtin⁵⁸, Y. Skovpen⁵⁸

Institute for High Energy Physics of National Research Centre 'Kurchatov Institute', Protvino, Russia
I. Azhgirey, I. Bayshev, D. Elumakhov, V. Kachanov, D. Konstantinov, P. Mandrik, V. Petrov, R. Ryutin, S. Slabospitskii, A. Sobol, S. Troshin, N. Tyurin, A. Uzunian, A. Volkov

National Research Tomsk Polytechnic University, Tomsk, Russia
A. Babaev, V. Okhotnikov

Tomsk State University, Tomsk, Russia
V. Borshch, V. Ivanchenko, E. Tcherniaev

University of Belgrade: Faculty of Physics and VINCA Institute of Nuclear Sciences, Belgrade, Serbia

P. Adzic⁵⁹, M. Dordevic, P. Milenovic, J. Milosevic

Centro de Investigaciones Energéticas Medioambientales y Tecnológicas (CIEMAT), Madrid, Spain

M. Aguilar-Benitez, J. Alcaraz Maestre, A. Álvarez Fernández, I. Bachiller, M. Barrio Luna, Cristina F. Bedoya, C.A. Carrillo Montoya, M. Cepeda, M. Cerrada, N. Colino, B. De La Cruz, A. Delgado Peris, J.P. Fernández Ramos, J. Flix, M.C. Fouz, O. Gonzalez Lopez, S. Goy Lopez, J.M. Hernandez, M.I. Josa, J. León Holgado, D. Moran, Á. Navarro Tobar, A. Pérez-Calero Yzquierdo, J. Puerta Pelayo, I. Redondo, L. Romero, S. Sánchez Navas, L. Urda Gómez, C. Willmott

Universidad Autónoma de Madrid, Madrid, Spain

J.F. de Trocóniz, R. Reyes-Almanza

Universidad de Oviedo, Instituto Universitario de Ciencias y Tecnologías Espaciales de Asturias (ICTEA), Oviedo, Spain

B. Alvarez Gonzalez, J. Cuevas, C. Erice, J. Fernandez Menendez, S. Folgueras, I. Gonzalez Caballero, J.R. González Fernández, E. Palencia Cortezon, C. Ramón Álvarez, J. Ripoll Sau, V. Rodríguez Bouza, A. Trapote, N. Trevisani

Instituto de Física de Cantabria (IFCA), CSIC-Universidad de Cantabria, Santander, Spain

J.A. Brochero Cifuentes, I.J. Cabrillo, A. Calderon, J. Duarte Campderros, M. Fernandez, C. Fernandez Madrazo, P.J. Fernández Manteca, A. García Alonso, G. Gomez, C. Martinez Rivero, P. Martinez Ruiz del Arbol, F. Matorras, P. Matorras Cuevas, J. Piedra Gomez, C. Prieels, T. Rodrigo, A. Ruiz-Jimeno, L. Scodellaro, I. Vila, J.M. Vizan Garcia

University of Colombo, Colombo, Sri Lanka

MK Jayananda, B. Kailasapathy⁶⁰, D.U.J. Sonnadara, DDC Wickramarathna

University of Ruhuna, Department of Physics, Matara, Sri Lanka

W.G.D. Dharmaratna, K. Liyanage, N. Perera, N. Wickramage

CERN, European Organization for Nuclear Research, Geneva, Switzerland

T.K. Aarrestad, D. Abbaneo, J. Alimena, E. Auffray, G. Auzinger, J. Baechler, P. Baillon[†], D. Barney, J. Bendavid, M. Bianco, A. Bocci, T. Camporesi, M. Capeans Garrido, G. Cerminara, S.S. Chhibra, L. Cristella, D. d'Enterria, A. Dabrowski, N. Daci, A. David, A. De Roeck, M.M. Defranchis, M. Deile, M. Dobson, M. Dünser, N. Dupont, A. Elliott-Peisert, N. Emriskova, F. Fallavollita⁶¹, D. Fasanella, S. Fiorendi, A. Florent, G. Franzoni, W. Funk, S. Giani, D. Gigi, K. Gill, F. Glege, L. Gouskos, M. Haranko, J. Hegeman, Y. Iiyama, V. Innocente, T. James, P. Janot, J. Kaspar, J. Kieseler, M. Komm, N. Kratochwil, C. Lange, S. Laurila, P. Lecoq, K. Long, C. Lourenço, L. Malgeri, S. Mallios, M. Mannelli, A.C. Marini, F. Meijers, S. Mersi, E. Meschi, F. Moortgat, M. Mulders, S. Orfanelli, L. Orsini, F. Pantaleo, L. Pape, E. Perez, M. Peruzzi, A. Petrilli, G. Petrucciani, A. Pfeiffer, M. Pierini, D. Piparo, M. Pitt, H. Qu, T. Quast, D. Rabady, A. Racz, G. Reales Gutiérrez, M. Rieger, M. Rovere, H. Sakulin, J. Salfeld-Nebgen, S. Scarfi, C. Schäfer, C. Schwick, M. Selvaggi, A. Sharma, P. Silva, W. Snoeys, P. Sphicas⁶², S. Summers, V.R. Tavolaro, D. Treille, A. Tsiros, G.P. Van Onsem, M. Verzetti, J. Wanczyk⁶³, K.A. Wozniak, W.D. Zeuner

Paul Scherrer Institut, Villigen, Switzerland

L. Caminada⁶⁴, A. Ebrahimi, W. Erdmann, R. Horisberger, Q. Ingram, H.C. Kaestli, D. Kotlinski, U. Langenegger, M. Missiroli, T. Rohe

ETH Zurich - Institute for Particle Physics and Astrophysics (IPA), Zurich, Switzerland

K. Androsov⁶³, M. Backhaus, P. Berger, A. Calandri, N. Chernyavskaya, A. De Cosa, G. Dissertori, M. Dittmar, M. Donegà, C. Dorfer, F. Eble, K. Gedia, F. Glessgen, T.A. Gómez Espinosa, C. Grab, D. Hits, W. Lusterhmann, A.-M. Lyon, R.A. Manzoni, C. Martin Perez, M.T. Meinhard, F. Nessi-Tedaldi, J. Niedziela, F. Pauss, V. Perovic, S. Pigazzini, M.G. Ratti, M. Reichmann, C. Reissel, T. Reitenspiess, B. Ristic, D. Ruini, D.A. Sanz Becerra, M. Schönenberger, V. Stampf, J. Steggemann⁶³, R. Wallny, D.H. Zhu

Universität Zürich, Zurich, Switzerland

C. Amsler⁶⁵, P. Bäertschi, C. Botta, D. Brzhechko, M.F. Canelli, K. Cormier, A. De Wit, R. Del Burgo, J.K. Heikkilä, M. Huwiler, A. Jofrehei, B. Kilminster, S. Leontsinis, A. Macchiolo, P. Meiring, V.M. Mikuni, U. Molinatti, I. Neutelings, A. Reimers, P. Robmann, S. Sanchez Cruz, K. Schweiger, Y. Takahashi

National Central University, Chung-Li, Taiwan

C. Adloff⁶⁶, C.M. Kuo, W. Lin, A. Roy, T. Sarkar³⁶, S.S. Yu

National Taiwan University (NTU), Taipei, Taiwan

L. Ceard, Y. Chao, K.F. Chen, P.H. Chen, W.-S. Hou, Y.y. Li, R.-S. Lu, E. Paganis, A. Psallidas, A. Steen, H.y. Wu, E. Yazgan, P.r. Yu

Chulalongkorn University, Faculty of Science, Department of Physics, Bangkok, Thailand

B. Asavapibhop, C. Asawatangtrakuldee, N. Srimanobhas

Çukurova University, Physics Department, Science and Art Faculty, Adana, Turkey

F. Boran, S. Damarseckin⁶⁷, Z.S. Demiroglu, F. Dolek, I. Dumanoglu⁶⁸, E. Eskut, Y. Guler, E. Gurpinar Guler⁶⁹, I. Hos⁷⁰, C. Isik, O. Kara, A. Kayis Topaksu, U. Kiminsu, G. Onengut, K. Ozdemir⁷¹, A. Polatoz, A.E. Simsek, B. Tali⁷², U.G. Tok, S. Turkcapar, I.S. Zorbakir, C. Zorbilmez

Middle East Technical University, Physics Department, Ankara, Turkey

B. Isildak⁷³, G. Karapinar⁷⁴, K. Ocalan⁷⁵, M. Yalvac⁷⁶

Bogazici University, Istanbul, Turkey

B. Akgun, I.O. Atakisi, E. Gülmez, M. Kaya⁷⁷, O. Kaya⁷⁸, Ö. Özçelik, S. Tekten⁷⁹, E.A. Yetkin⁸⁰

Istanbul Technical University, Istanbul, Turkey

A. Cakir, K. Cankocak⁶⁸, Y. Komurcu, S. Sen⁸¹

Istanbul University, Istanbul, Turkey

S. Cerci⁷², B. Kaynak, S. Ozkorucuklu, D. Sunar Cerci⁷²

Institute for Scintillation Materials of National Academy of Science of Ukraine, Kharkov, Ukraine

B. Grynyov

National Scientific Center, Kharkov Institute of Physics and Technology, Kharkov, Ukraine

L. Levchuk

University of Bristol, Bristol, United Kingdom

D. Anthony, E. Bhal, S. Bologna, J.J. Brooke, A. Bundock, E. Clement, D. Cussans, H. Flacher, J. Goldstein, G.P. Heath, H.F. Heath, M.I. Holmberg⁸², L. Kreczko, B. Krikler, S. Paramesvaran, S. Seif El Nasr-Storey, V.J. Smith, N. Stylianou⁸³, K. Walkingshaw Pass, R. White

Rutherford Appleton Laboratory, Didcot, United Kingdom

K.W. Bell, A. Belyaev⁸⁴, C. Brew, R.M. Brown, D.J.A. Cockerill, C. Cooke, K.V. Ellis, K. Harder,

S. Harper, J. Linacre, K. Manolopoulos, D.M. Newbold, E. Olaiya, D. Petyt, T. Reis, T. Schuh, C.H. Shepherd-Themistocleous, I.R. Tomalin, T. Williams

Imperial College, London, United Kingdom

R. Bainbridge, P. Bloch, S. Bonomally, J. Borg, S. Breeze, O. Buchmuller, V. Cepaitis, G.S. Chahal⁸⁵, D. Colling, P. Dauncey, G. Davies, M. Della Negra, S. Fayer, G. Fedi, G. Hall, M.H. Hassanshahi, G. Iles, J. Langford, L. Lyons, A.-M. Magnan, S. Malik, A. Martelli, D.G. Monk, J. Nash⁸⁶, M. Pesaresi, D.M. Raymond, A. Richards, A. Rose, E. Scott, C. Seez, A. Shtipliyski, A. Tapper, K. Uchida, T. Virdee¹⁹, M. Vojinovic, N. Wardle, S.N. Webb, D. Winterbottom, A.G. Zecchinelli

Brunel University, Uxbridge, United Kingdom

K. Coldham, J.E. Cole, A. Khan, P. Kyberd, I.D. Reid, L. Teodorescu, S. Zahid

Baylor University, Waco, USA

S. Abdullin, A. Brinkerhoff, B. Caraway, J. Dittmann, K. Hatakeyama, A.R. Kanuganti, B. McMaster, N. Pastika, M. Saunders, S. Sawant, C. Sutantawibul, J. Wilson

Catholic University of America, Washington, DC, USA

R. Bartek, A. Dominguez, R. Uniyal, A.M. Vargas Hernandez

The University of Alabama, Tuscaloosa, USA

A. Buccilli, S.I. Cooper, D. Di Croce, S.V. Gleyzer, C. Henderson, C.U. Perez, P. Rumerio⁸⁷, C. West

Boston University, Boston, USA

A. Akpınar, A. Albert, D. Arcaro, C. Cosby, Z. Demiragli, E. Fontanesi, D. Gastler, J. Rohlf, K. Salyer, D. Sperka, D. Spitzbart, I. Suarez, A. Tsatsos, S. Yuan, D. Zou

Brown University, Providence, USA

G. Benelli, B. Burkley, X. Coubez²⁰, D. Cutts, M. Hadley, U. Heintz, J.M. Hogan⁸⁸, G. Landsberg, K.T. Lau, M. Lukasik, J. Luo, M. Narain, S. Sagir⁸⁹, E. Usai, W.Y. Wong, X. Yan, D. Yu, W. Zhang

University of California, Davis, Davis, USA

J. Bonilla, C. Brainerd, R. Breedon, M. Calderon De La Barca Sanchez, M. Chertok, J. Conway, P.T. Cox, R. Erbacher, G. Haza, F. Jensen, O. Kukral, R. Lander, M. Mulhearn, D. Pellett, B. Regnery, D. Taylor, Y. Yao, F. Zhang

University of California, Los Angeles, USA

M. Bachtis, R. Cousins, A. Datta, D. Hamilton, J. Hauser, M. Ignatenko, M.A. Iqbal, T. Lam, W.A. Nash, S. Regnard, D. Saltzberg, B. Stone, V. Valuev

University of California, Riverside, Riverside, USA

K. Burt, Y. Chen, R. Clare, J.W. Gary, M. Gordon, G. Hanson, G. Karapostoli, O.R. Long, N. Mangano, M. Olmedo Negrete, W. Si, S. Wimpenny, Y. Zhang

University of California, San Diego, La Jolla, USA

J.G. Branson, P. Chang, S. Cittolin, S. Cooperstein, N. Deelen, D. Diaz, J. Duarte, R. Gerosa, L. Giannini, D. Gilbert, J. Guiang, R. Kansal, V. Krutelyov, R. Lee, J. Letts, M. Masciovecchio, S. May, M. Pieri, B.V. Sathia Narayanan, V. Sharma, M. Tadel, A. Vartak, F. Würthwein, Y. Xiang, A. Yagil

University of California, Santa Barbara - Department of Physics, Santa Barbara, USA

N. Amin, C. Campagnari, M. Citron, A. Dorsett, V. Dutta, J. Incandela, M. Kilpatrick, J. Kim, B. Marsh, H. Mei, M. Oshiro, M. Quinnan, J. Richman, U. Sarica, J. Sheplock, D. Stuart, S. Wang

California Institute of Technology, Pasadena, USA

A. Bornheim, O. Cerri, I. Dutta, J.M. Lawhorn, N. Lu, J. Mao, H.B. Newman, J. Ngadiuba, T.Q. Nguyen, M. Spiropulu, J.R. Vlimant, C. Wang, S. Xie, Z. Zhang, R.Y. Zhu

Carnegie Mellon University, Pittsburgh, USA

J. Alison, S. An, M.B. Andrews, P. Bryant, T. Ferguson, A. Harilal, C. Liu, T. Mudholkar, M. Paulini, A. Sanchez

University of Colorado Boulder, Boulder, USA

J.P. Cumalat, W.T. Ford, A. Hassani, E. MacDonald, R. Patel, A. Perloff, C. Savard, K. Stenson, K.A. Ulmer, S.R. Wagner

Cornell University, Ithaca, USA

J. Alexander, S. Bright-thonney, Y. Cheng, D.J. Cranshaw, S. Hogan, J. Monroy, J.R. Patterson, D. Quach, J. Reichert, M. Reid, A. Ryd, W. Sun, J. Thom, P. Wittich, R. Zou

Fermi National Accelerator Laboratory, Batavia, USA

M. Albrow, M. Alyari, G. Apollinari, A. Apresyan, A. Apyan, S. Banerjee, L.A.T. Bauerdick, D. Berry, J. Berryhill, P.C. Bhat, K. Burkett, J.N. Butler, A. Canepa, G.B. Cerati, H.W.K. Cheung, F. Chlebana, M. Cremonesi, K.F. Di Petrillo, V.D. Elvira, Y. Feng, J. Freeman, Z. Gecse, L. Gray, D. Green, S. Grünendahl, O. Gutsche, R.M. Harris, R. Heller, T.C. Herwig, J. Hirschauer, B. Jayatilaka, S. Jindariani, M. Johnson, U. Joshi, T. Klijnsma, B. Klima, K.H.M. Kwok, S. Lammel, D. Lincoln, R. Lipton, T. Liu, C. Madrid, K. Maeshima, C. Mantilla, D. Mason, P. McBride, P. Merkel, S. Mrenna, S. Nahn, V. O'Dell, V. Papadimitriou, K. Pedro, C. Pena⁵⁷, O. Prokofyev, F. Ravera, A. Reinsvold Hall, L. Ristori, B. Schneider, E. Sexton-Kennedy, N. Smith, A. Soha, W.J. Spalding, L. Spiegel, S. Stoynev, J. Strait, L. Taylor, S. Tkaczyk, N.V. Tran, L. Uplegger, E.W. Vaandering, H.A. Weber

University of Florida, Gainesville, USA

D. Acosta, P. Avery, D. Bourilkov, L. Cadamuro, V. Cherepanov, F. Errico, R.D. Field, D. Guerrero, B.M. Joshi, M. Kim, E. Koenig, J. Konigsberg, A. Korytov, K.H. Lo, K. Matchev, N. Menendez, G. Mitselmakher, A. Muthirakalayil Madhu, N. Rawal, D. Rosenzweig, S. Rosenzweig, K. Shi, J. Sturdy, J. Wang, E. Yigitbasi, X. Zuo

Florida State University, Tallahassee, USA

T. Adams, A. Askew, R. Habibullah, V. Hagopian, K.F. Johnson, R. Khurana, T. Kolberg, G. Martinez, H. Prosper, C. Schiber, O. Viazlo, R. Yohay, J. Zhang

Florida Institute of Technology, Melbourne, USA

M.M. Baarmand, S. Butalla, T. Elkafrawy⁹⁰, M. Hohlmann, R. Kumar Verma, D. Noonan, M. Rahmani, F. Yumiceva

University of Illinois at Chicago (UIC), Chicago, USA

M.R. Adams, H. Becerril Gonzalez, R. Cavanaugh, X. Chen, S. Dittmer, O. Evdokimov, C.E. Gerber, D.A. Hangal, D.J. Hofman, A.H. Merrit, C. Mills, G. Oh, T. Roy, S. Rudrabhatla, M.B. Tonjes, N. Varelas, J. Viinikainen, X. Wang, Z. Wu, Z. Ye

The University of Iowa, Iowa City, USA

M. Alhusseini, K. Dilsiz⁹¹, R.P. Gandrajula, O.K. Köseyan, J.-P. Merlo, A. Mestvirishvili⁹², J. Nachtman, H. Ogul⁹³, Y. Onel, A. Penzo, C. Snyder, E. Tiras⁹⁴

Johns Hopkins University, Baltimore, USA

O. Amram, B. Blumenfeld, L. Corcodilos, J. Davis, M. Eminizer, A.V. Gritsan, S. Kyriacou, P. Maksimovic, J. Roskes, M. Swartz, T.Á. Vámi

The University of Kansas, Lawrence, USA

A. Abreu, J. Anguiano, C. Baldenegro Barrera, P. Baringer, A. Bean, A. Bylinkin, Z. Flowers, T. Isidori, S. Khalil, J. King, G. Krintiras, A. Kropivnitskaya, M. Lazarovits, C. Lindsey, J. Marquez, N. Minafra, M. Murray, M. Nickel, C. Rogan, C. Royon, R. Salvatico, S. Sanders, E. Schmitz, C. Smith, J.D. Tapia Takaki, Q. Wang, Z. Warner, J. Williams, G. Wilson

Kansas State University, Manhattan, USA

S. Duric, A. Ivanov, K. Kaadze, D. Kim, Y. Maravin, T. Mitchell, A. Modak, K. Nam

Lawrence Livermore National Laboratory, Livermore, USA

F. Rebassoo, D. Wright

University of Maryland, College Park, USA

E. Adams, A. Baden, O. Baron, A. Belloni, S.C. Eno, N.J. Hadley, S. Jabeen, R.G. Kellogg, T. Koeth, A.C. Mignerey, S. Nabili, M. Seidel, A. Skuja, L. Wang, K. Wong

Massachusetts Institute of Technology, Cambridge, USA

D. Abercrombie, G. Andreassi, R. Bi, S. Brandt, W. Busza, I.A. Cali, Y. Chen, M. D'Alfonso, J. Eysermans, C. Freer, G. Gomez Ceballos, M. Goncharov, P. Harris, M. Hu, M. Klute, D. Kovalskyi, J. Krupa, Y.-J. Lee, B. Maier, C. Mironov, C. Paus, D. Rankin, C. Roland, G. Roland, Z. Shi, G.S.F. Stephans, K. Tatar, J. Wang, Z. Wang, B. Wyslouch

University of Minnesota, Minneapolis, USA

R.M. Chatterjee, A. Evans, P. Hansen, J. Hiltbrand, Sh. Jain, M. Krohn, Y. Kubota, J. Mans, M. Revering, R. Rusack, R. Saradhy, N. Schroeder, N. Strobbe, M.A. Wadud

University of Nebraska-Lincoln, Lincoln, USA

K. Bloom, M. Bryson, S. Chauhan, D.R. Claes, C. Fangmeier, L. Finco, F. Golf, C. Joo, I. Kravchenko, M. Musich, I. Reed, J.E. Siado, G.R. Snow[†], W. Tabb, F. Yan

State University of New York at Buffalo, Buffalo, USA

G. Agarwal, H. Bandyopadhyay, L. Hay, I. Iashvili, A. Kharchilava, C. McLean, D. Nguyen, J. Pekkanen, S. Rappoccio, A. Williams

Northeastern University, Boston, USA

G. Alverson, E. Barberis, Y. Haddad, A. Hortiangtham, J. Li, G. Madigan, B. Marzocchi, D.M. Morse, V. Nguyen, T. Orimoto, A. Parker, L. Skinnari, A. Tishelman-Charny, T. Wamorkar, B. Wang, A. Wisecarver, D. Wood

Northwestern University, Evanston, USA

S. Bhattacharya, J. Bueghly, Z. Chen, A. Gilbert, T. Gunter, K.A. Hahn, Y. Liu, N. Odell, M.H. Schmitt, M. Velasco

University of Notre Dame, Notre Dame, USA

R. Band, R. Bucci, A. Das, N. Dev, R. Goldouzian, M. Hildreth, K. Hurtado Anampa, C. Jessop, K. Lannon, J. Lawrence, N. Loukas, D. Lutton, N. Marinelli, I. Mcalister, T. McCauley, F. Meng, K. Mohrman, Y. Musienko⁴⁹, R. Ruchti, P. Siddireddy, A. Townsend, M. Wayne, A. Wightman, M. Wolf, M. Zarucki, L. Zygala

The Ohio State University, Columbus, USA

B. Bylsma, B. Cardwell, L.S. Durkin, B. Francis, C. Hill, M. Nunez Ornelas, K. Wei, B.L. Winer, B.R. Yates

Princeton University, Princeton, USA

F.M. Addesa, B. Bonham, P. Das, G. Dezoort, P. Elmer, A. Frankenthal, B. Greenberg,

N. Haubrich, S. Higginbotham, A. Kalogeropoulos, G. Kopp, S. Kwan, D. Lange, M.T. Lucchini, D. Marlow, K. Mei, I. Ojalvo, J. Olsen, C. Palmer, D. Stickland, C. Tully

University of Puerto Rico, Mayaguez, USA

S. Malik, S. Norberg

Purdue University, West Lafayette, USA

A.S. Bakshi, V.E. Barnes, R. Chawla, S. Das, L. Gutay, M. Jones, A.W. Jung, S. Karmarkar, M. Liu, G. Negro, N. Neumeister, G. Paspalaki, C.C. Peng, S. Piperov, A. Purohit, J.F. Schulte, M. Stojanovic¹⁵, J. Thieman, F. Wang, R. Xiao, W. Xie

Purdue University Northwest, Hammond, USA

J. Dolen, N. Parashar

Rice University, Houston, USA

A. Baty, M. Decaro, S. Dildick, K.M. Ecklund, S. Freed, P. Gardner, F.J.M. Geurts, A. Kumar, W. Li, B.P. Padley, R. Redjimi, W. Shi, A.G. Stahl Leitton, S. Yang, L. Zhang, Y. Zhang

University of Rochester, Rochester, USA

A. Bodek, P. de Barbaro, R. Demina, J.L. Dulemba, C. Fallon, T. Ferbel, M. Galanti, A. Garcia-Bellido, O. Hindrichs, A. Khukhunaishvili, E. Ranken, R. Taus

Rutgers, The State University of New Jersey, Piscataway, USA

B. Chiarito, J.P. Chou, A. Gandrakota, Y. Gershtein, E. Halkiadakis, A. Hart, M. Heindl, O. Karacheban²³, I. Laflotte, A. Lath, R. Montalvo, K. Nash, M. Osherson, S. Salur, S. Schnetzer, S. Somalwar, R. Stone, S.A. Thayil, S. Thomas, H. Wang

University of Tennessee, Knoxville, USA

H. Acharya, A.G. Delannoy, S. Spanier

Texas A&M University, College Station, USA

O. Bouhali⁹⁵, M. Dalchenko, A. Delgado, R. Eusebi, J. Gilmore, T. Huang, T. Kamon⁹⁶, H. Kim, S. Luo, S. Malhotra, R. Mueller, D. Overton, D. Rathjens, A. Safonov

Texas Tech University, Lubbock, USA

N. Akchurin, J. Damgov, V. Hegde, S. Kunori, K. Lamichhane, S.W. Lee, T. Mengke, S. Muthumuni, T. Peltola, I. Volobouev, Z. Wang, A. Whitbeck

Vanderbilt University, Nashville, USA

E. Appelt, S. Greene, A. Gurrola, W. Johns, A. Melo, H. Ni, K. Padeken, F. Romeo, P. Sheldon, S. Tuo, J. Velkovska

University of Virginia, Charlottesville, USA

M.W. Arenton, B. Cox, G. Cummings, J. Hakala, R. Hirosky, M. Joyce, A. Ledovskoy, A. Li, C. Neu, B. Tannenwald, S. White, E. Wolfe

Wayne State University, Detroit, USA

R. Harr, N. Poudyal

University of Wisconsin - Madison, Madison, WI, USA

K. Black, T. Bose, J. Buchanan, C. Caillol, S. Dasu, I. De Bruyn, P. Everaerts, F. Fienga, C. Galloni, H. He, M. Herndon, A. Hervé, U. Hussain, A. Lanaro, A. Loeliger, R. Loveless, J. Madhusudanan Sreekala, A. Mallampalli, A. Mohammadi, D. Pinna, A. Savin, V. Shang, V. Sharma, W.H. Smith, D. Teague, S. Trembath-reichert, W. Vetens

†: Deceased

- 1: Also at TU Wien, Wien, Austria
- 2: Also at Institute of Basic and Applied Sciences, Faculty of Engineering, Arab Academy for Science, Technology and Maritime Transport, Alexandria, Egypt, Alexandria, Egypt
- 3: Also at Université Libre de Bruxelles, Bruxelles, Belgium
- 4: Also at Universidade Estadual de Campinas, Campinas, Brazil
- 5: Also at Federal University of Rio Grande do Sul, Porto Alegre, Brazil
- 6: Also at University of Chinese Academy of Sciences, Beijing, China
- 7: Also at Department of Physics, Tsinghua University, Beijing, China, Beijing, China
- 8: Also at UFMS, Nova Andradina, Brazil
- 9: Also at Nanjing Normal University Department of Physics, Nanjing, China
- 10: Now at The University of Iowa, Iowa City, USA
- 11: Also at Institute for Theoretical and Experimental Physics named by A.I. Alikhanov of NRC 'Kurchatov Institute', Moscow, Russia
- 12: Also at Joint Institute for Nuclear Research, Dubna, Russia
- 13: Also at Cairo University, Cairo, Egypt
- 14: Also at Zewail City of Science and Technology, Zewail, Egypt
- 15: Also at Purdue University, West Lafayette, USA
- 16: Also at Université de Haute Alsace, Mulhouse, France
- 17: Also at Tbilisi State University, Tbilisi, Georgia
- 18: Also at Erzincan Binali Yildirim University, Erzincan, Turkey
- 19: Also at CERN, European Organization for Nuclear Research, Geneva, Switzerland
- 20: Also at RWTH Aachen University, III. Physikalisches Institut A, Aachen, Germany
- 21: Also at University of Hamburg, Hamburg, Germany
- 22: Also at Department of Physics, Isfahan University of Technology, Isfahan, Iran, Isfahan, Iran
- 23: Also at Brandenburg University of Technology, Cottbus, Germany
- 24: Also at Skobeltsyn Institute of Nuclear Physics, Lomonosov Moscow State University, Moscow, Russia
- 25: Also at Physics Department, Faculty of Science, Assiut University, Assiut, Egypt
- 26: Also at Karoly Robert Campus, MATE Institute of Technology, Gyongyos, Hungary
- 27: Also at Institute of Physics, University of Debrecen, Debrecen, Hungary, Debrecen, Hungary
- 28: Also at Institute of Nuclear Research ATOMKI, Debrecen, Hungary
- 29: Also at MTA-ELTE Lendület CMS Particle and Nuclear Physics Group, Eötvös Loránd University, Budapest, Hungary, Budapest, Hungary
- 30: Also at Wigner Research Centre for Physics, Budapest, Hungary
- 31: Also at IIT Bhubaneswar, Bhubaneswar, India, Bhubaneswar, India
- 32: Also at Institute of Physics, Bhubaneswar, India
- 33: Also at G.H.G. Khalsa College, Punjab, India
- 34: Also at Shoolini University, Solan, India
- 35: Also at University of Hyderabad, Hyderabad, India
- 36: Also at University of Visva-Bharati, Santiniketan, India
- 37: Also at Indian Institute of Technology (IIT), Mumbai, India
- 38: Also at Deutsches Elektronen-Synchrotron, Hamburg, Germany
- 39: Also at Sharif University of Technology, Tehran, Iran
- 40: Also at Department of Physics, University of Science and Technology of Mazandaran, Behshahr, Iran
- 41: Now at INFN Sezione di Bari ^a, Università di Bari ^b, Politecnico di Bari ^c, Bari, Italy

-
- 42: Also at Italian National Agency for New Technologies, Energy and Sustainable Economic Development, Bologna, Italy
- 43: Also at Centro Siciliano di Fisica Nucleare e di Struttura Della Materia, Catania, Italy
- 44: Also at Università di Napoli 'Federico II', NAPOLI, Italy
- 45: Also at Consiglio Nazionale delle Ricerche - Istituto Officina dei Materiali, PERUGIA, Italy
- 46: Also at Riga Technical University, Riga, Latvia, Riga, Latvia
- 47: Also at Consejo Nacional de Ciencia y Tecnología, Mexico City, Mexico
- 48: Also at IRFU, CEA, Université Paris-Saclay, Gif-sur-Yvette, France
- 49: Also at Institute for Nuclear Research, Moscow, Russia
- 50: Now at National Research Nuclear University 'Moscow Engineering Physics Institute' (MEPhI), Moscow, Russia
- 51: Also at Institute of Nuclear Physics of the Uzbekistan Academy of Sciences, Tashkent, Uzbekistan
- 52: Also at St. Petersburg State Polytechnical University, St. Petersburg, Russia
- 53: Also at University of Florida, Gainesville, USA
- 54: Also at Imperial College, London, United Kingdom
- 55: Also at P.N. Lebedev Physical Institute, Moscow, Russia
- 56: Also at Moscow Institute of Physics and Technology, Moscow, Russia, Moscow, Russia
- 57: Also at California Institute of Technology, Pasadena, USA
- 58: Also at Budker Institute of Nuclear Physics, Novosibirsk, Russia
- 59: Also at Faculty of Physics, University of Belgrade, Belgrade, Serbia
- 60: Also at Trincomalee Campus, Eastern University, Sri Lanka, Nilaveli, Sri Lanka
- 61: Also at INFN Sezione di Pavia ^a, Università di Pavia ^b, Pavia, Italy, Pavia, Italy
- 62: Also at National and Kapodistrian University of Athens, Athens, Greece
- 63: Also at Ecole Polytechnique Fédérale Lausanne, Lausanne, Switzerland
- 64: Also at Universität Zürich, Zurich, Switzerland
- 65: Also at Stefan Meyer Institute for Subatomic Physics, Vienna, Austria, Vienna, Austria
- 66: Also at Laboratoire d'Annecy-le-Vieux de Physique des Particules, IN2P3-CNRS, Annecy-le-Vieux, France
- 67: Also at Şırnak University, Sirnak, Turkey
- 68: Also at Near East University, Research Center of Experimental Health Science, Nicosia, Turkey
- 69: Also at Konya Technical University, Konya, Turkey
- 70: Also at Istanbul University - Cerrahpasa, Faculty of Engineering, Istanbul, Turkey
- 71: Also at Piri Reis University, Istanbul, Turkey
- 72: Also at Adiyaman University, Adiyaman, Turkey
- 73: Also at Ozyegin University, Istanbul, Turkey
- 74: Also at Izmir Institute of Technology, Izmir, Turkey
- 75: Also at Necmettin Erbakan University, Konya, Turkey
- 76: Also at Bozok Universitetesi Rektörlüğü, Yozgat, Turkey, Yozgat, Turkey
- 77: Also at Marmara University, Istanbul, Turkey
- 78: Also at Milli Savunma University, Istanbul, Turkey
- 79: Also at Kafkas University, Kars, Turkey
- 80: Also at Istanbul Bilgi University, Istanbul, Turkey
- 81: Also at Hacettepe University, Ankara, Turkey
- 82: Also at Rutherford Appleton Laboratory, Didcot, United Kingdom
- 83: Also at Vrije Universiteit Brussel, Brussel, Belgium
- 84: Also at School of Physics and Astronomy, University of Southampton, Southampton, United Kingdom

- 85: Also at IPPP Durham University, Durham, United Kingdom
- 86: Also at Monash University, Faculty of Science, Clayton, Australia
- 87: Also at Università di Torino, TORINO, Italy
- 88: Also at Bethel University, St. Paul, Minneapolis, USA, St. Paul, USA
- 89: Also at Karamanoğlu Mehmetbey University, Karaman, Turkey
- 90: Also at Ain Shams University, Cairo, Egypt
- 91: Also at Bingol University, Bingol, Turkey
- 92: Also at Georgian Technical University, Tbilisi, Georgia
- 93: Also at Sinop University, Sinop, Turkey
- 94: Also at Erciyes University, KAYSERI, Turkey
- 95: Also at Texas A&M University at Qatar, Doha, Qatar
- 96: Also at Kyungpook National University, Daegu, Korea, Daegu, Korea